

Robert Granhei
Emma Victoria Vinje Græsno

Green Ironmaking - Carburization of Green Direct Reduced Iron (DRI)

Reduksjon av jernoksid-pellets i hydrogen

Projectnumber: IMA-B-14-2023
Assignee: IMA/NTNU
Contact person: Prof. Ragnhild E. Aune

Bachelor's thesis in Chemical Engineering

Supervisor: Ragnhild Elizabeth Aune

Co-supervisor: Mårten Grönerup

Submission date: 10 June 2023

Norwegian University of Science and Technology

Faculty of Natural Sciences

Department of Material Science and Engineering



ABSTRACT

Current commercial means of ironmaking rely heavily on using the Blast Furnace (BF) technology, which produces a lot of CO₂ emissions every year with coke as one of the raw materials together with the iron ore. A greener alternative to the BF process is the Direct Reduction of Iron (DRI) process, which uses reductive gases, such as H₂ and CO, to remove the oxygen from the iron ore, making it suitable for steel production. The emissions from the DRI process are dramatically lower than the BF process, ranging from about 42 % to 5 % of the CO₂ emissions produced by the BF/BOF process.

The present work aimed to investigate the optimum temperature for reducing iron ore pellets by a mixture of 50% H₂ gas and 50% Ar gas at varying temperatures (570 °C, 670 °C and 770 °C). Furthermore, the reduced iron ore pellets were also to be carburised in an atmosphere of CH₄ gas. The reduction and carburisation processes were performed in a high-temperature vacuum furnace in the temperature interval 25 °C - 770 °C, and the processes were also simulated using the HSC Chemistry 9 software from Metso Outotec.

The experiments performed in the high-temperature vacuum furnace resulted in iron ore pellets that showed increased porosity, indicating that the reduction process had been initiated. Most of the reduced pellets also revealed a decrease in oxygen concentration at the surface, except the pellets reduced at 770 °C, which might be due to re-oxidation of the pellet surface before analysis. The pellets carburised at 670 °C and 770 °C showed complete carburisation, but the sample carburised at 570 °C showed a clear difference between two layers that had and had not been carburised. It was concluded that this temperature was too low for obtaining successful carburisation.

The process simulations using HSC Chemistry 9 showed a complete reduction and carburisation of an average iron ore pellet with the given parameters. As the software assumes equilibrium at every step, as well as the fact that all pellet contains a certain level of inhomogeneity, only indications of what to expect can be obtained. In view of this, the simulation results proved to be in good agreement with the overall outcome of the experimental work.

Keywords: Iron ore, Ironmaking, Direct Reduction of Iron (DRI), Blast Furnace, Carburisation, HSC Chemistry 9

SAMMENDRAG

Dagens mest vanlige måte å lage jern fra jernmalm på er ved bruk av masovn, som produserer en stor mengde CO₂-utslipp hvert år. Et grønnere alternativ til masovn er Direkte Reduksjon av Jern (DRI), som bruker reduksjonsgasser, som H₂ og CO, til å fjerne oksyget fra jernmalmen, som gjør jernet egnet for stålproduksjon. Utslippene til DRI-prosessen er mye lavere enn ved bruk av masovn, med en mengde på kun 42 % til 5 % av CO₂ utslippet til masovnplassen.

Dette arbeidet hadde som mål å finne optimal temperatur for reduksjon av jernmalm-pellets i en blanding av 50% H₂ og 50% Ar ved varierende temperaturer (570 °C, 670 °C og 770 °C). I tillegg ble de reduserte jernmalm-pelletsene også karburisert i en atmosfære bestående av CH₄-gass. Reduksjons- og karburiseringsprosessen ble utført i en høy-temperatur vakuumovn i temperaturintervallet 25 °C - 770 °C, og prosessene ble også simulert ved bruk av programvaren HSC Chemistry 9 fra Metso Outotec.

Forsøkene gjort på høy-temperatur vakuumovnen resulterte i jernmalm-pellets som viste mer porøsitet, en indikasjon på at reduksjonsprosessen hadde startet. De fleste prøvene viste også en nedgang i oksygenkonsentrasjon, bortsett fra pelleten redusert ved 770 °C, noe som kan være på grunn av reoskivering av overflaten til pelleten før analyse. Pelletene karburert ved 670 °C og 770 °C viste en fullstendig karburisering, men prøven karburert ved 570 °C viste et tydelig skille mellom to lag som hadde og hadde ikke blitt karburert. Det ble konkludert at denne temperaturen var for lav for å oppnå en fullstendig karburisering.

Prosesssimuleringene gjort i HSC Chemistry 9 viste en fullstendig reduksjon og karburisering av en gjennomsnittlig pellet med de gitte parameterne. Siden programvaren antar likevekt ved hvert trinn, og siden alle pellets er, til en viss grad, inhomogene, er det bare indikasjoner på hva som kan forventes som oppnås. I lys av dette viste det seg at simulasjonsresultatene stemte godt overens med de overordnede resultatene fra det eksperimentelle arbeidet.

Nøkkelord: Jernmalm, Jernlagning, Direkte Reduksjon av Jern (DRI), Masovn, Karburisering, HSC Chemistry 9.

PREFACE

The present thesis, entitled “Green Ironmaking – Carburization of Green Direct Reduced Iron (DRI)”, comprises an overview of the work performed by reducing iron ore pellets in an atmosphere of H_2 gas and CO gas at varying temperatures followed by carburisation in an atmosphere of CH_4 gas. The initial plan was to perform all experiments using Thermogravimetric Analyses (TGA). However, due to instrumental failure (gas leakage), the experimental part of the work was performed in a High-temperature Vacuum Furnace instead using a mixture of H_2 gas and Ar gas as the reducing agent.

The work was coordinated through the Department of Material Science and Engineering (IMA) at the Norwegian University of Science and Technology (NTNU) in Trondheim, Norway, with support from Aker Horizons, Oslo, Norway.

ACKNOWLEDGEMENT

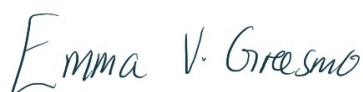
The present authors would first and foremost like to thank their supervisor, Prof. Ragnhild E. Aune, for all the help she has provided us. Despite numerous problems during the experimental part of the work, they did eventually cross the finish line, which was only possible with her support. They would also like to thank their external supervisor, Dr. Mårten Görnerup at Aker Horizons, for his insights and knowledge that helped them along the way.

A special thanks to the Department of Material Science and Engineering (IMA) at NTNU, Campus Gløshaugen in Trondheim, Norway, for giving access to their laboratories, as well as the excellent training and guidance received from the department's engineers Ruben Åge Hansen and Yingda Yu. Last but not least, thank you to Amalie My Olsen for her support with the TGA apparatus and the HSC Chemistry software, as well as Dr. Sarina Bao from Sintef Industry for training in running the high-temperature vacuum furnace.

Trondheim 10.06.23



Robert Granhei



Emma Victoria V. Græsmo

CONTENTS

1	Introduction	1
1.1	Objectives	3
2	Background	5
2.1	Blast Furnace (BF) Process	5
2.2	Direct Reduced Iron (DRI) Process	6
2.3	Carburisation	7
3	Theory	9
3.1	The Shrinking Core Model	9
4	Material, Experimental Method and Analytical Approach	13
4.1	Iron ore pellets	13
4.2	Experimental Method 1 - Thermogravimetric Analysis (TGA) . . .	14
4.3	Experimental Method 2 - High-temperature vacuum furnace	16
4.4	Analytical approach - Scanning Electron Microscope (SEM) with Energy Dispersive Spectroscopy (EDS)	17
4.4.1	Sample Preparation	18
4.5	HSC Chemistry	19
5	Results and Discussion	21
5.1	Experimental method 1 – Thermogravimetric analysis (TGA) . . .	21
5.2	Experimental method 2 - High Temperature Vacuum Furnace . . .	24
5.3	HSC Chemistry 9	33
6	Summary & Conclusions	35
7	Future Work	37
	References	39
	Appendices:	42
	Appendix A - Sample preparation	43
	Appendix B - SEM/EDS Analysis	45
	Appendix C - HSC Chemistry 9 Calculations	49

INTRODUCTION

Iron and steel production plays an essential role worldwide, with a total mass of 1 878.5 Mt (million tonnes) produced in 2022 [1]. The production of iron and steel does, however, come with a significant drawback in view of the CO₂ emissions connected to these metallurgical processes. In 2018, it was estimated that 71% of the global steel production came from the pig iron produced in the Blast Furnaces (BF), which was further refined in the Basic Oxygen Furnaces (BOF), producing 1 279 Mt of steel [2]. Compared to other alternative iron-making technologies, the BF produces a copious amount of CO₂ during iron production [3]. This is because, in the BF/BOF operations, coke reduces the oxygen from the iron ore, and CO₂ is produced as a side product. Like any other type of CO₂ emission, the BF/BOF operations passively contribute to environmental problems like global warming, destabilising ecosystems, poor air quality, human and animal health risks, etc. [4].

Figure 1.0.1 presents the worldwide crude steel production for 2022, with circles indicating the total steel produced per country [5]. The demand for steel is forecasted to increase by 0.1% during the beginning of 2023 and continue to grow throughout the year to a production corresponding to 1 822.3 Mt of steel produced during 2023 [6]. The World Steel Association also anticipates a continued growth trend into 2024, forecasting a 1.7% increase in steel demand, corresponding to 1 854 Mt [7].

An alternative, more eco-friendly method of producing pig iron does exist, i.e. the technology behind Direct Reduced Iron (DRI). In this process, the oxide is directly reduced from the iron ore by a reducing gas atmosphere, e.g., by H₂ gas, CO gas, or a mixture of these gases. The reduced iron produced through this method is used in the Electric Arc Furnace (EAF) to produce steel. The DRI/EAF processes are key counterparts to the BF/BOF processes to reach the United Nation's (UN's) CO₂ footprint goals [8] [9]. Although the DRI/EAF processes emit CO₂, the emissions are considerably less than in the case of BF/BOF processes [10].

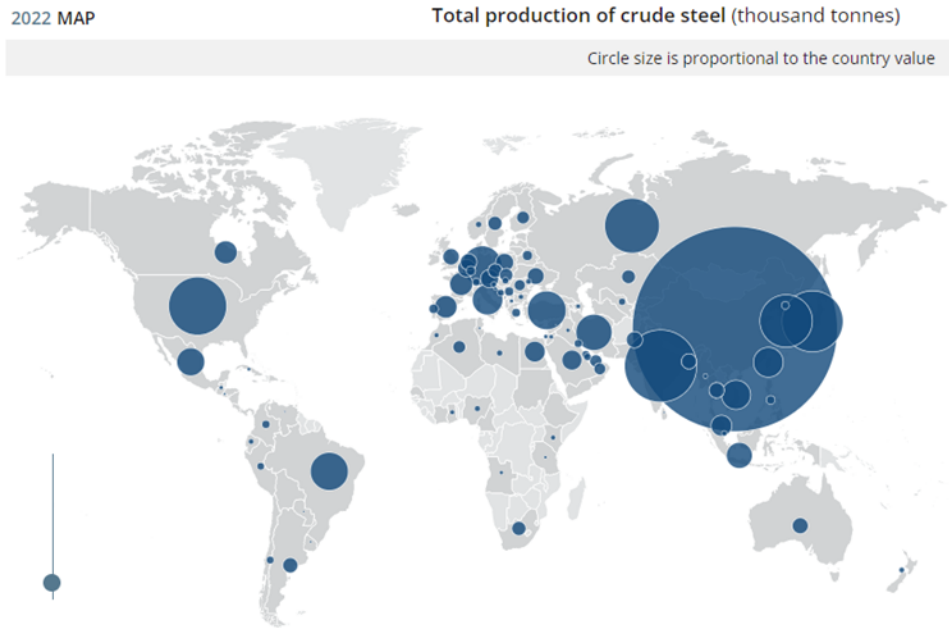


Figure 1.0.1: The crude steel production worldwide, with circles indicating the proportion produced per country during 2022 [5].

A factor that affects the amount of CO_2 emission from the DRI/EAF processes is the types of reducing agents used. Examples of reducing agents are natural gases, which are said to emit only 42% of the carbon emission from the BF/BOF processes. Other processes, like hydrogen electrolysis, are reported to emit only 5% [10].

Scaling up the DRI industry would be favourable, but it would also prove challenging due to the huge investments required. It would necessitate extensive changes in infrastructure, which will also require time, effort, and financial resources. Another problem is the reducing agents used. Most producers of DRI would prefer to use pure hydrogen, however, its use in the DRI/EAF industry is currently scarce and are yet to be prioritised on full scale [11].

There are several publications and MSc/PhD theses on the topic of DRI with the aim of finding the most efficient way to reduce and carburise iron ore pellets, using different reducing agents. In the study by Beheshti et al. [12], it was stated that experiments with better temperature control were of future interest.

1.1 Objectives

The present work intends to clarify the influence of temperature on the reduction of iron ore pellets through the DRI process using H_2 as the reducing agent, as well as securing a low carbon content in the final product. The specific objectives for the present work have, based on this, been to:

- Reduce iron ore pellets at varying temperatures and establish the optimal reduction temperature.
- Carburise the reduced iron ore pellet with a carbon-rich gas (CH_4).
- Utilise the “Equilibrium Compositions”-module of the HSC Chemistry 9 software to simulate the reduction and carburisation processes adapted to iron ore pellets in the DRI process.

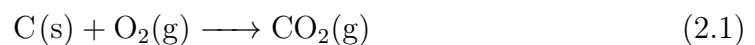
BACKGROUND

The iron ore extracted from the earth is not pure iron, but different iron oxides, of which the most common ones are hematite (Fe_2O_3), magnetite (Fe_3O_4), limonite ($2\text{Fe}_2\text{O}_3 \cdot 3\text{H}_2\text{O}$) and siderite (FeCO_3) [13]. In order to use these oxides as raw material in the production of iron, the oxygen in the ore needs to be liberated through an iron-making process. The most common of the iron-making processes is the BF process, but the Direct Reduction (DR) method can also be used.

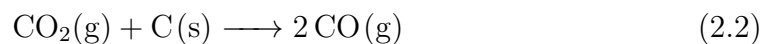
2.1 Blast Furnace (BF) Process

The BF is a counter-current gas-solid reactor where the raw materials, i.e., iron ore, coke, and limestone, descend through a column filled with ascending hot gases. This process is continuous with raw materials being fed in, and molten iron and slag being tapped out from the bottom of the reactor [14]. The BF process is illustrated in Figure 2.1.1.

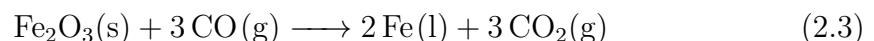
The reactor is supplied with hot air rich in oxygen. The coke added to the furnace will react with the oxygen in the air, creating CO_2 , as shown in Equation (2.1).



The CO_2 will further react with the coke, creating CO , as in Equation (2.2).



The CO will then act as a reducing agent for the iron ore, liberating the iron from the oxygen, illustrated in Equation (2.3).



Usually, an additive or a flux will be added to convert the waste or gangue materials in the reactants into a slag with a low melting point that can also dissolve the coke ash and remove any sulphur. Limestone is a common additive used in the BF process for this purpose. At higher temperatures, limestone will decompose into calcium oxide and CO_2 . This is shown in Equation (2.4).

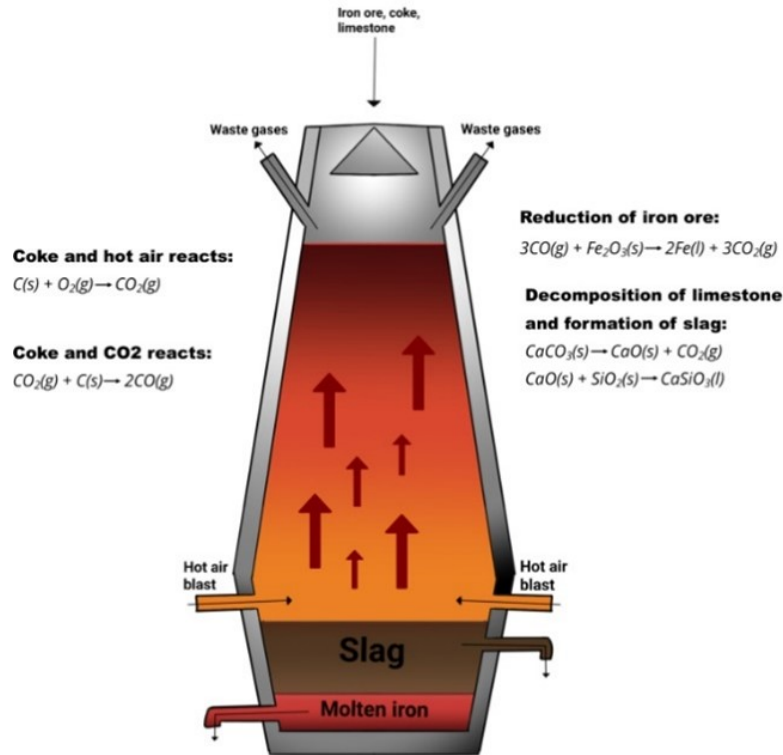
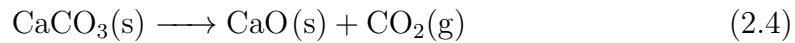
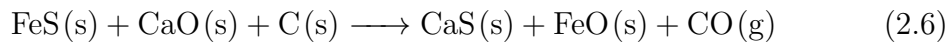


Figure 2.1.1: Illustration of the BF process for the production of pig iron.



The calcium oxide will then create a slag with unwanted materials, as in Equations (2.5) and (2.6).



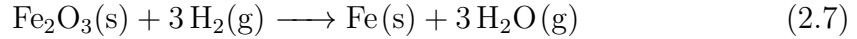
There are several advantages to using the BF for the production of pig iron, as the process is continuous, highly efficient, suitable for large-scale productions, and it is a relatively low-cost production. Also, the process is widely used worldwide, meaning the technology is well-developed and available. There are also disadvantages to using BF process due to the CO_2 emissions, as well as the need for high-quality raw materials, which can be challenging to acquire, and it consumes a considerable amount of energy [15].

2.2 Direct Reduced Iron (DRI) Process

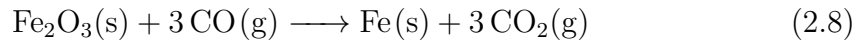
DRI, also called sponge iron, is the product of the DR of iron ore. The reduction process is a solid-state reaction process, i.e., solid-solid or solid-gas reaction, where removable oxygen is eliminated from the iron oxide. Because the oxygen is

removed, the iron becomes porous.

DR processes can be split into two groups based on what reductant is used to obtain the DRI, i.e., solid reductants (e.g., coal) or gaseous reductants [16]. An illustration of a DRI reactor is shown in Figure 2.2.1. Iron ore pellets are reduced to iron and the oxygen is removed with the help of reducing atmosphere (e.g., H_2 gas). The overall reaction is shown in Equ. (2.7). The oxygen reacts with hydrogen gas and iron, creating water vapour.



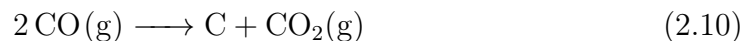
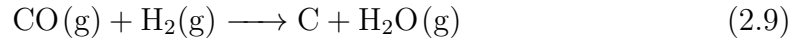
The reaction in Equ. (2.8) will also apply in the presence of CO gas. In this reaction, the oxygen reacts with the CO gas to create CO_2 gas.



The DRI process has several advantages, such as high energy efficiency. The process is also more environmentally friendly than the BF process, especially when H_2 gas is used as the reducing atmosphere. The main disadvantages of the process are that the DRI is susceptible to oxidation/corrosion and that it requires a large amount of natural gases during production, which can limit production in areas where natural gases are not available in the needed amounts [17] [18].

2.3 Carburisation

Carburisation is a heat treatment process where iron or steel absorbs carbon while the metal is heated in an atmosphere of a carbon-containing gas, such as CO or CH_4 . The carbon content in the product depends largely on the composition and temperature of the carbon-containing gases, as well as on the surface characteristics of the material. The reduction of iron ore by the DRI can be made in an atmosphere with only H_2 gas, following Equ. (2.7). However, it is desirable to have some presence of carbon in the DRI, as it offers several benefits when the DRI is used further in the EAF for the production of steel. Some of the advantages are securing a lower melting point of the metallic iron, reduced demand for electric energy, and avoidance of re-oxidation [19]. A carbon source should therefore be introduced in the reduction process. Equations (2.9) to (2.11) shows how carbon-containing gases are used to give carbon to the DRI, while Equation (2.12) is the carburisation reaction.



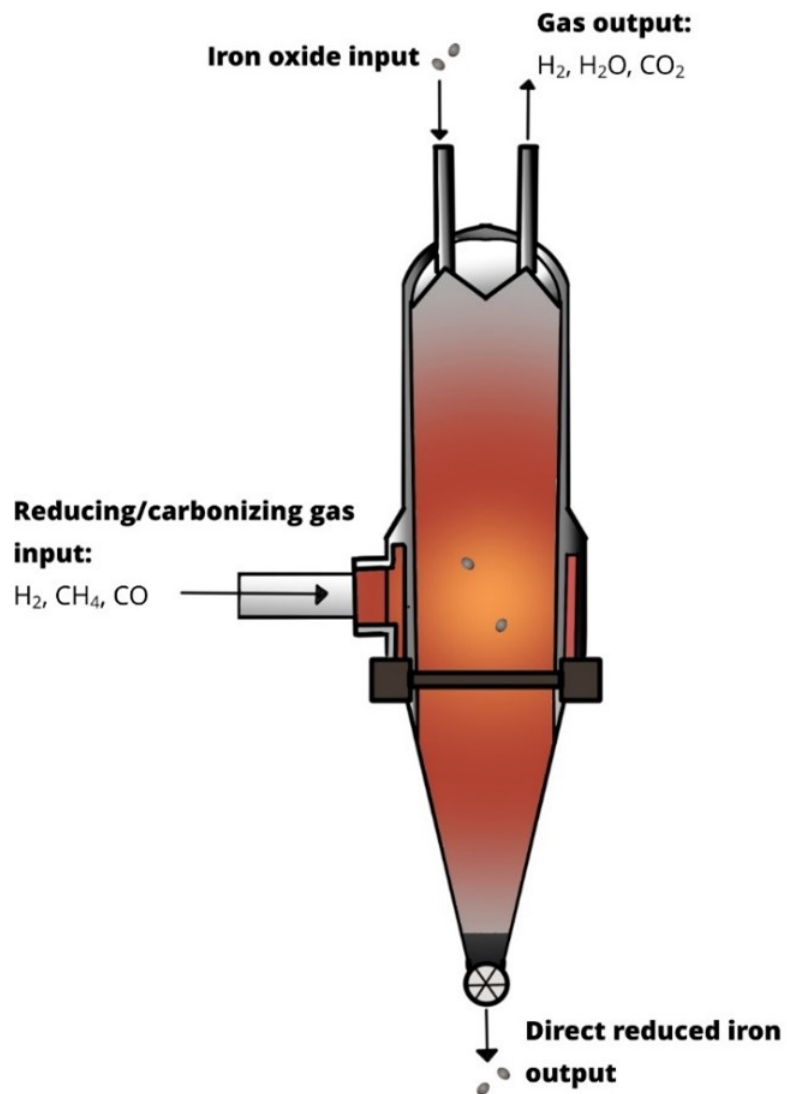


Figure 2.2.1: Illustration of a DRI reactor for the production of DRI.

The DR process is a solid-gas reaction where the solid Fe_2O_3 reacts with the gaseous H_2 , creating water vapour (H_2O) and reduced Fe. The iron ore pellets may vary in porosity and shape, but they are all roughly spherical with a 1-1.5 cm diameter. The precise reaction kinetics of the process is more complex than it may seem, as the reaction shown in Equ. (2.7) is not what immediately happens.

To model the kinetics of the reduction process of the iron ore pellet, there are three main categories [20]. The first is the heterogeneous model in which the porosity of the unreacted solid is negligible. It means that either the solid is impervious to the gaseous reactant, or the intrinsic reactivity of the solid is so high that the reaction occurs mainly in the zone near the surface. The shrinking core model is another example of a heterogeneous model. The second is the homogeneous model, which deals with highly porous materials, meaning that the gaseous reactant can pass freely and is available everywhere in the pellet. The reaction will therefore be happening throughout the material. This model is irrelevant to iron ore pellets, as they are not porous enough to fit the model. The last model is the intermediate model, which deals with material where the pore diffusion from the homogeneous model, as well as the resistance by a chemical reaction from the heterogeneous model are comparable. In this case, both models must be considered simultaneously. Although this model may be applied to iron ore pellets, the high degree of complexity makes this model challenging to work with.

3.1 The Shrinking Core Model

As mentioned, the shrinking core model is an example of a heterogeneous model for a solid-gas reaction. It describes situations where a solid particle is consumed, either by dissolution or reaction. The result is that the core made of the original material “shrinks” as the reduction proceeds. A cross-section of a reduced pellet may reveal layers made of the various intermediate steps in the reduction process, with the outer-most layers more reduced than the innermost, which is illustrated in Figure 3.1.1. To use the model, a few assumptions need to be considered.

- The pellet maintains a constant porosity.

- The bulk flow concentration and temperature remain constant.
- The gaseous flow velocity outside the pellet is constant.
- The pellet is spherical (the reaction does not change its diameter), and no cracks are formed on the surface.
- The chemical reaction taking place is irreversible and of the first order.

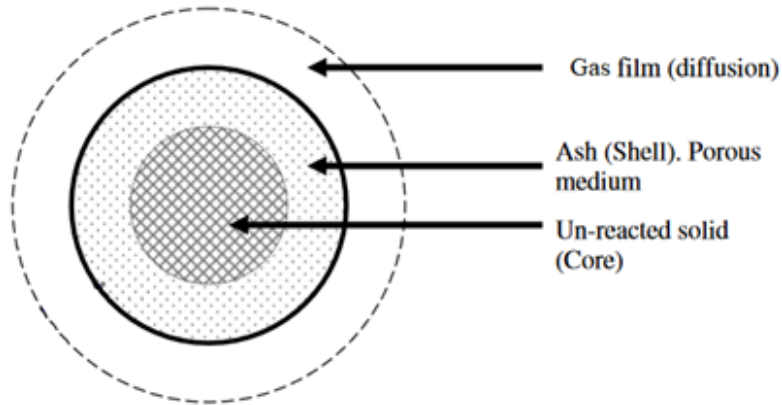
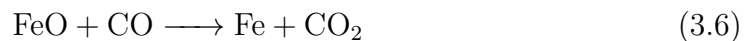
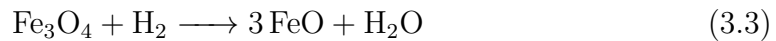
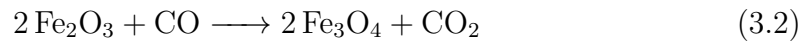
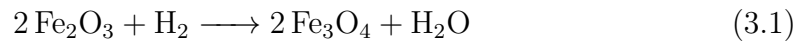


Figure 3.1.1: Illustration of the shrinking core model.

Equ. (2.7) and Equ. (2.8) are the overall reactions we are interested in for the reduction, but the complete process has several intermediate steps. As can be seen from Figure 3.1.2, the reduction process has three intermediate steps, i.e., the hematite (Fe_2O_3) reduces first to magnetite (Fe_3O_4), which further reduces to wüstite (FeO), which finally reduces to iron (Fe). The step-by-step reactions can be seen in Equ. (3.1) to (3.6). Many different factors can, however, influence the rate which these reactions occur, and overall, the kinetics can be very complex. Still, previous studies have shown that generally, higher temperatures give higher conversion rates [12] [21].



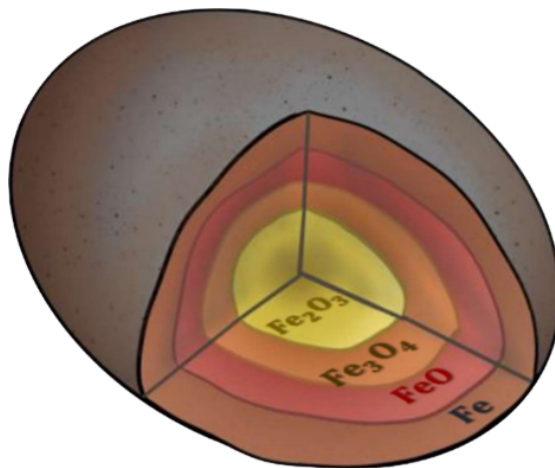


Figure 3.1.2: The shrinking core model for reducing Fe_2O_3 .

MATERIAL, EXPERIMENTAL METHOD AND
ANALYTICAL APPROACH

4.1 Iron ore pellets

Iron oxide pellets, depicted in Figure 4.1.1, are spherical iron concentrates. They possess a structure that makes them highly useful for metallurgical processes. Their compact yet porous form does not only give them efficient packing with other pellets, but also allows access to reacting gases to diffuse in the pellets, which in this case are the reducing and carbonizing gases that pass throughout the pellets. This allows them to be directly implemented into metallurgical processes.



Figure 4.1.1: Picture of an iron oxide pellet.

They are lightweight due to their approximately 20 - 30% porosity, and they typically weigh between 2 - 5 g [22]. While predominantly composed of iron, they contain traces of other elements like silica, calcium, and magnesium. For a more detailed breakdown of the iron oxide pellet elemental composition, refer to Table 4.1.1.

Table 4.1.1: Table of elemental composition of iron ore pellets used in this experiment in terms of weight.

Elements	Composition [%]
Fe	67.8
FeO	0.30
SiO ₂	0.80
CaO	0.90
MgO	0.65
Al ₂ O ₃	0.20
TiO ₂	0.18
V ₂ O ₅	0.20
MnO	0.07
Na ₂ O	0.03
K ₂ O	0.03
Cr	<0.002
Cu	<0.001
Ni	<0.03
P	0.025
S	<0.002
Zn	<0.003
F	<0.006
Cl	<0.002
Moisture	1.5

4.2 Experimental Method 1 - Thermogravimetric Analysis (TGA)

Thermogravimetric Analysis (TGA) was a method used in this experiment to simulate the thermal behaviour of samples by tracking changes in mass over time, known as "thermal stability" measurement. It does so by continuously weighing the sample using a microbalance [23] [24]. This happens in an enclosed furnace, with a given atmosphere, often by an inert gas like nitrogen or argon [25] [24]. When a material is being heated, its mass decreases as parts of the composition of the solids are converted to gas [23]. A mass loss curve will be generated as the heating process happens. The graph starts from left to right and commonly

provides the frequency of mass loss from the sample (m) in terms of the temperature (T) or time (t). The resulting graph is known as a Thermogravimetric curve (TG curve). It is widely used to quantify the mass change of both organic and inorganic samples [26]. In the context of a DR reactor, TGA serves as a smaller, laboratory-scale alternative that typically analyses one sample at a time.

The experiment utilized the Linseis™ TGA PT 1600© model, which consisted of a thermobalance (scale), a furnace, a thermocouple for temperature detection, an automatic recording unit for monitoring mass and temperature changes, a recorder, and a cooling system. These components come together to form the TGA device shown in Figure 4.2.1. The thermocouple used in this experiment was a Type-S (platinum–rhodium, alloy), which can support temperatures up to 1600 °C [27]. Before use, the thermocouple was calibrated to ensure there were no deviations from the indicated temperature. This calibration consisted of baselines done at 700 °C, 800 °C, and 900 °C.

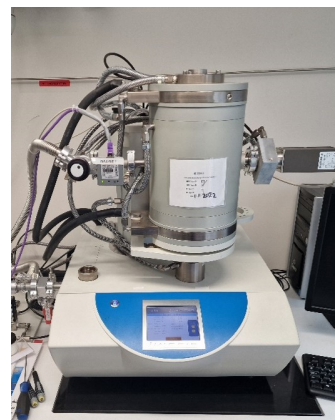


Figure 4.2.1: Picture of the Linseis™ TGA PT 1600© used in this experiment.

In this experiment, there was a focus on the oxidative and reductive reactions that caused mass loss between the samples and gases. Therefore, the experiment focused on running two sets of iron samples in parallel: one set consisted of reduced samples, while the other set comprised of samples that were both reduced and carburised. The aim was to analyse these iron pellets at temperatures of 700 °C, 800 °C, and 900 °C in an atmosphere of H_2 and CO . During the carburisation experiments, CH_4 gas was used during the cooling phase. This allowed for a comparison of the effects of reduction and carburisation in both sample sets.

The heating process was conducted quasistatic, involving variations between isothermal and dynamic temperatures [23]. The process started by gradually increasing the temperature with an atmosphere of inert argon until it reached the desired level, followed by a period of isothermal temperature, where the H_2 and CO gas was added to the TGA holder to start the reduction. Afterwards, the temperature decreased back to room temperature. For the carburisation experiments, the CH_4 gas was filled into the chamber during the cooling process. For more information regarding the specific temperature program, see Table 4.2.1.

Given the substantial duration of the process, the samples were selected to remain small enough for the reacting gases to diffuse while still being suitable for further analysis. Therefore, the samples in this experiment maintained a short diameter of approximately 1 to 1.5 cm and a mass ranging from 2 to 4 g.

Table 4.2.1: Temperature program used for the TGA experiments. The reduction process happens in step 2 when the TGA has reached peak temperature, and the carburisation happens during the cooling process in step 3.

Step	Temperature rate [°C/min]	Set temperature [°C]	Dwell time
1	15	300	30
2	5	700/800/900	160
3	5	300	60
4	15	20	-

4.3 Experimental Method 2 - High-temperature vacuum furnace

A high-temperature vacuum furnace was also used to run experiments. This was done as a supplement to the experiments done on the TGA, as the furnace experiments takes a lot less time. The experimental setup was the same: two parallels of samples, one with only reduction and one with reduction and carburisation, were done at temperatures of 700 °C, 800 °C and 900°C. The furnace consists of an inner and outer chamber and does not have a balance, so there is no way to track changes to the sample while the experiment is running. The thermocouple used was a Type - C (tungsten - rhenium alloy), which supports temperatures up to 2300 °C [28]. A calibration was done during the experimental phase to ascertain whether the thermocouple temperature deviated from the actual temperature in the furnace. This was done by melting a copper piece in the furnace and comparing its measured melting point with its theoretical, which is 1085 °C. A deviation was found, and an additional experiment was conducted where the set temperature was adjusted for the deviation.

The furnace is pictured in Figure 4.3.1. The samples used for this furnace ranged in mass from 2.648 g to 3.534 g. To start the experiment, a sample is placed on the flat crucible of the furnace. To minimize the risk of the sample falling off the crucible during the process, the bottom side of the pellet is sanded down a little to make it flatter. Then, the crucible with the sample is slowly and carefully pushed into the inner chamber of the furnace, where it will be for the duration of the experiment.

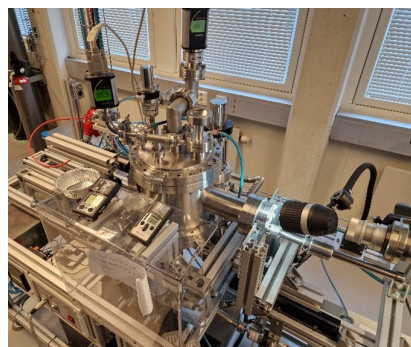


Figure 4.3.1: The high-temperature vacuum furnace utilized.

The temperature program used is shown in Table 4.3.1. Before starting the heating process, the furnace is vacuumed and refilled with H₂ gas. The furnace is heated at a rate of 100 °C/min up to set peak temperature, that it holds for 160 min. The furnace main-

tains the hydrogen atmosphere for the duration of the reduction process. Once the reduction is complete, the cooling phase begins. In the reduction-only experiments, this phase happened very quickly, but for the carburisation experiments, the cooling must be more controlled. First, an extra 10 minutes are added to step 2. During these 10 minutes, the furnace is vacuumed and refilled with CH_4 gas. Then, the cooling phase is done at a rate of $25^\circ\text{C}/\text{min}$ down to room temperature.

Table 4.3.1: Temperature program used for the TGA experiments. The reduction process happens in step 2 when the TGA has reached max. temperature, and the carburisation happens during the cooling process in step 3.

Step	Time [min]	Start temperature [$^\circ\text{C}$]	End temperature [$^\circ\text{C}$]	Gas flow [L/min]
1	7/8/9	25	700/800/900	H_2 : 0.1
2	160	700/800/900	Unchanged	H_2 : 0.1
3	5 27/31/35	700/800/900	25	Ar: 1 CH_4 : 0.1

4.4 Analytical approach - Scanning Electron Microscope (SEM) with Energy Dispersive Spectroscopy (EDS)

Scanning Electron Microscope (SEM) is an electron microscope that was utilized to examine the sample's surface on a microscale. Despite the light microscope, which can be viewed at a magnitude limit of 1500 times, SEM can examine samples at a substantially higher scale, at about 100 000 times with high-resolution images [29] [30]. The SEM is one of the electron microscopes, where the first was invented in 1931 by Ernest Ruska and Max Knoll, Germany [31]. However, the first Scanning Electron Microscope was invented in 1937, by Manfred Von Ardenne, Germany [31]. The Zeiss Ultra 55 SEM was used in this experiment. It offers high-resolution imaging and supports elemental mapping, which makes it suitable for analyzing iron samples [32].

When SEM was used, some samples had to be coated in gold ions, which assured conductivity and consequently emits secondary electrons [33]. The SEM used an electron gun that offshoots an "electron beam" which through deflections reached the sample and emitted secondary electrons from it, which were detected by a secondary electron detector that visualized the surface of the sample. Electrons from the incident electron beam that scatters back to the detector, hence the name backscatter electrons, visualized the deeper regions of the sample [34]. With an integrated magnetic lens, the generated picture from the electrons was showcased by adjusting zoom and focus. Pictures were rendered as colourless black-and-white photos, where the surface was brighter from the secondary electrons, and the deeper regions from the backscattered electrons appeared darker [34].

The SEM offered EDS (Energy Dispersive Spectroscopy), a form of chemical analysis [35]. EDS offered a mapping of every element distribution on the surface of the sample. Therefore, the detection of carbon was conveniently done to determine if the sample had been carbonized. Other contaminations were detected as well. In the case of this experiment, iron will be examined. Thus, it was expected to detect impurities such as oxides and metals.

The Zeiss Ultra 55 SEM was used in this experiment. It offered high-resolution imaging and supported elemental mapping, which made it suitable for analyzing iron samples. The preparation involved multiple steps, this included cutting the pellets in half, casting them in epoxy, and then polishing them. The array of samples set for analysis consisted of an unreduced sample, a TGA reduced sample at 700 °C, reduced samples at 570 °C, 670 °C and 770 °C, and both reduced and carburised samples at 570 °C, 670 °C, 770 °C and 800 °C.

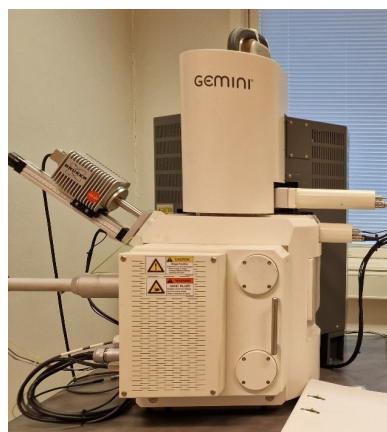


Figure 4.4.1: Picture of The Zeiss Ultra 55 SEM.

The analytical methods conducted with this device were taking detailed SEM images, performing elemental analysis, and elemental mapping (EDS). SEM imaging was taken with two magnitudes: 1000 X and 8000 X. The elemental analysis primarily targeted the central regions of the samples, aimed at identifying the specific elements presented in that region. The EDS procedure was utilized to analyse the dispersion of iron, the reduction implications of oxygen, and carbon for the carburisation effects within the samples.

4.4.1 Sample Preparation

Before the sample was examined in the SEM, it had to be properly and carefully prepared. After the sample was reduced, it had to be cut open to analyse the core on a flat surface. Cutting the sample in half left scratches and saw marks on the surface, which would obfuscate the sample when using the SEM. Any contamination would also obscure the SEM photos and had to be removed during the sample pre-treatment. Therefore, the sample's surface had to be thoroughly polished to ensure that the surface looked even in the SEM. This was performed by using multiple grinding plates bearing different degrees of granularity. A full overview of the sample preparation is given in Appendix A. Lastly, if necessary, the sample is covered with an ionic gold coating, which as mentioned bears the emitting secondary electrons for samples that are not conductive, which was the case for the unreduced sample. The chamber containing the sample must be vacuumed before starting the examination, this is because electrons travel faster in such an atmosphere [36].

4.5 HSC Chemistry

HSC Chemistry 9 (HSC) is a computer software distributed by Outotec that can be used to simulate chemical processes and perform thermodynamic calculations [37]. The module used in this project was Equilibrium Composition. This module is used to simulate the composition of a heterogeneous multi-component system when equilibrium is reached. To do this, the chemical reaction system needs to be defined, i.e., the phases and species assumed to be present in the system, the amounts of initial raw material, and the temperature of the process. The module uses the Gibbs free energy minimizing method to calculate equilibrium compositions. The results can be plotted as a function of temperature partial pressure, etc. It is worth noting that the module assumes equilibrium at every temperature, which is unrealistic in a practical setting.

Equilibrium Compositions will be used in this thesis to simulate the reduction and carburisation processes. The equations used will be Equation 2.7 for the reduction and Equations 2.11 and 2.12 combined for the carburisation. The input amounts for the reduction are based on the experiments done in the high-temperature vacuum furnace detailed in 4.3. The initial amount of iron in the carburisation is taken from the results of the reduction simulation.

RESULTS AND DISCUSSION

5.1 Experimental method 1 – Thermogravimetric analysis (TGA)

During the experiments with the TGA, it was discovered that the machine was leaking gas. Due to the dangerous gases used, the experiment was stopped, and further experiments with the TGA was cancelled. Therefore, there are not a lot of results to show for the TGA.

The graph in Figure 5.1.1 shows the interrupted experiment. Set temperature for the reduction was 700 °C. The green graph is for the mass change of the sample. As the figure shows, the reduction process starts immediately when the reducing gases are added, and the mass change is quite dramatic. The pellet had a mass of 4.793 g before the reduction, and in only a few minutes, the pellet lost around 0.580 g. This is a mass change of 12%.

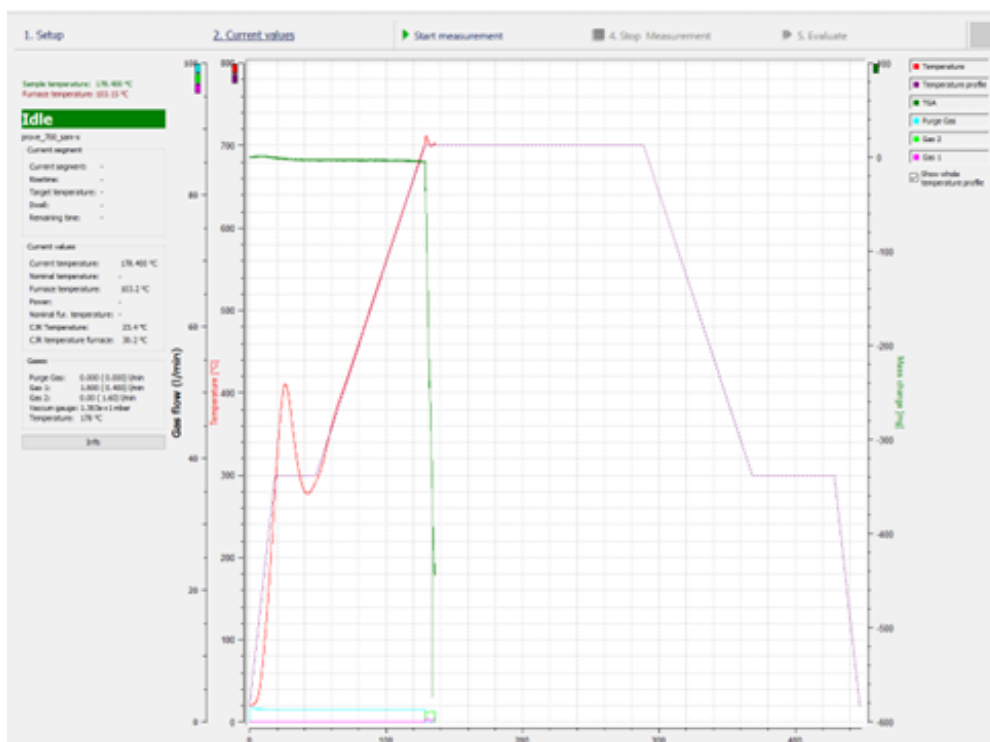
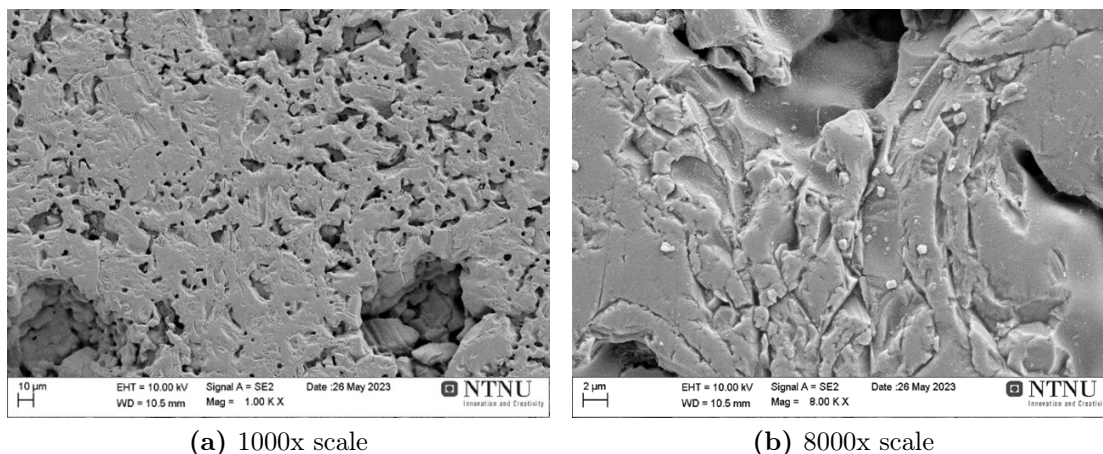


Figure 5.1.1: The graph of the interrupted experiment.

The pellet from this experiment was analysed in SEM. Figure 5.1.2 shows pictures of an unreduced pellet and Figure 5.1.3 is from the pellet reduced in the interrupted TGA-experiment. The reduced sample shows a small increase in porosity, which is to be expected, even though the experiment ended prematurely. In addition, the small white impurities shown in Figure 5.1.2 (b) are not present in the reduced sample.



(a) 1000x scale

(b) 8000x scale

Figure 5.1.2: Surface structure of unreduced sample.

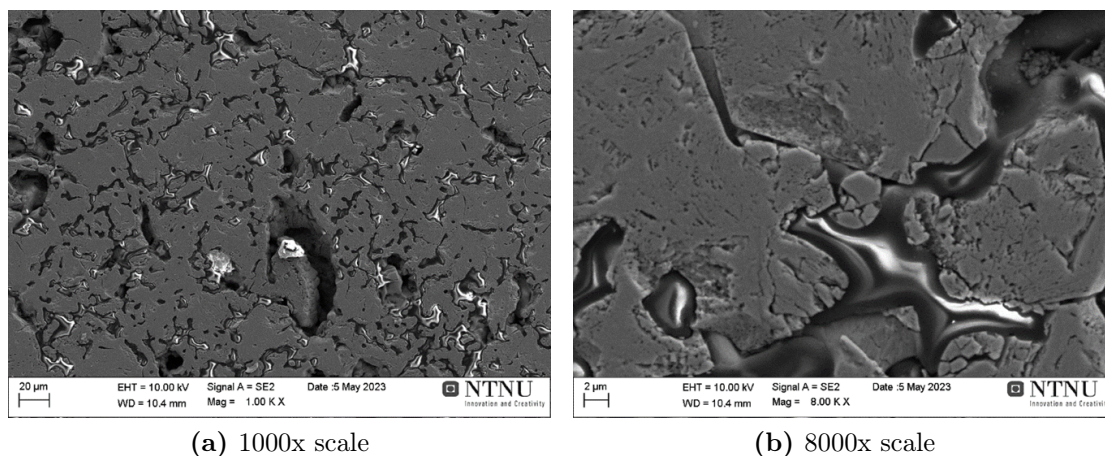


Figure 5.1.3: Surface structure of sample reduced in TGA.

An elemental mapping was done on the unreduced and the TGA pellet. This is shown in Figures 5.1.4 and 5.1.5. The mapping shows that the TGA pellet is still rich in oxygen, which is expected because the experiment was stopped very early. Had the experiment been allowed to continue, it would be expected that the oxygen content decreased. Because CO gas was also used in the experiment, the carbon content might also have increased slightly compared to the unreduced sample.

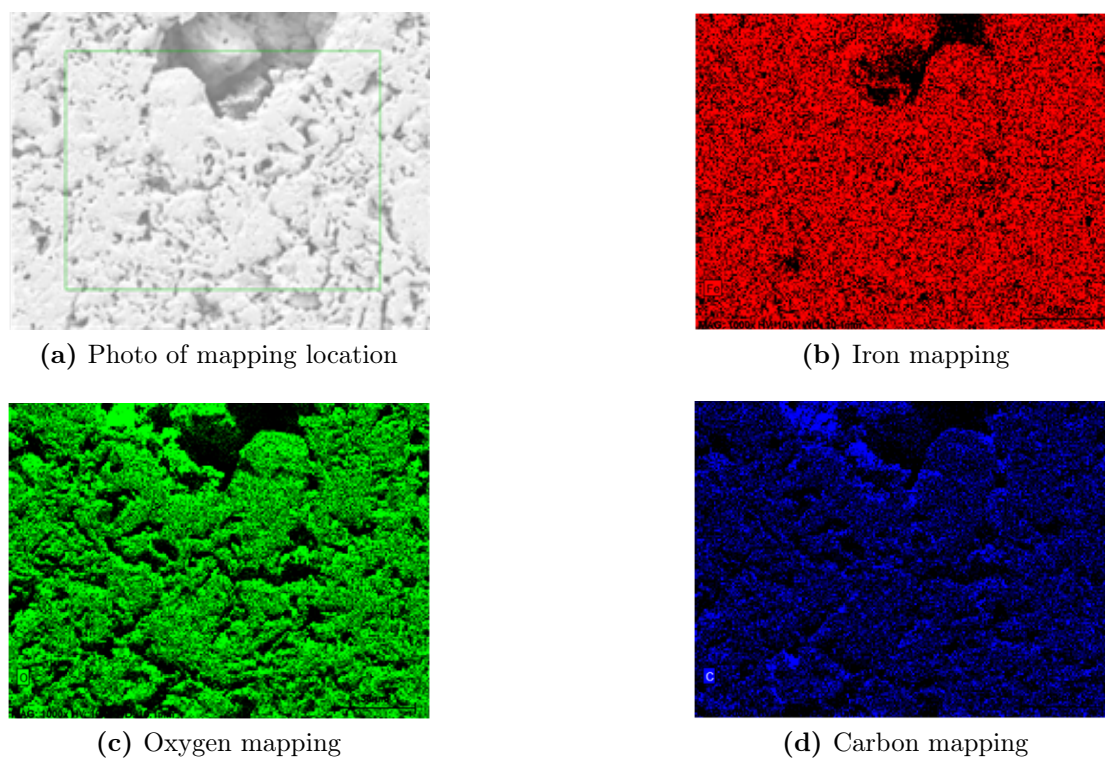


Figure 5.1.4: Elemental mapping of an unreduced sample. 1000x scale.

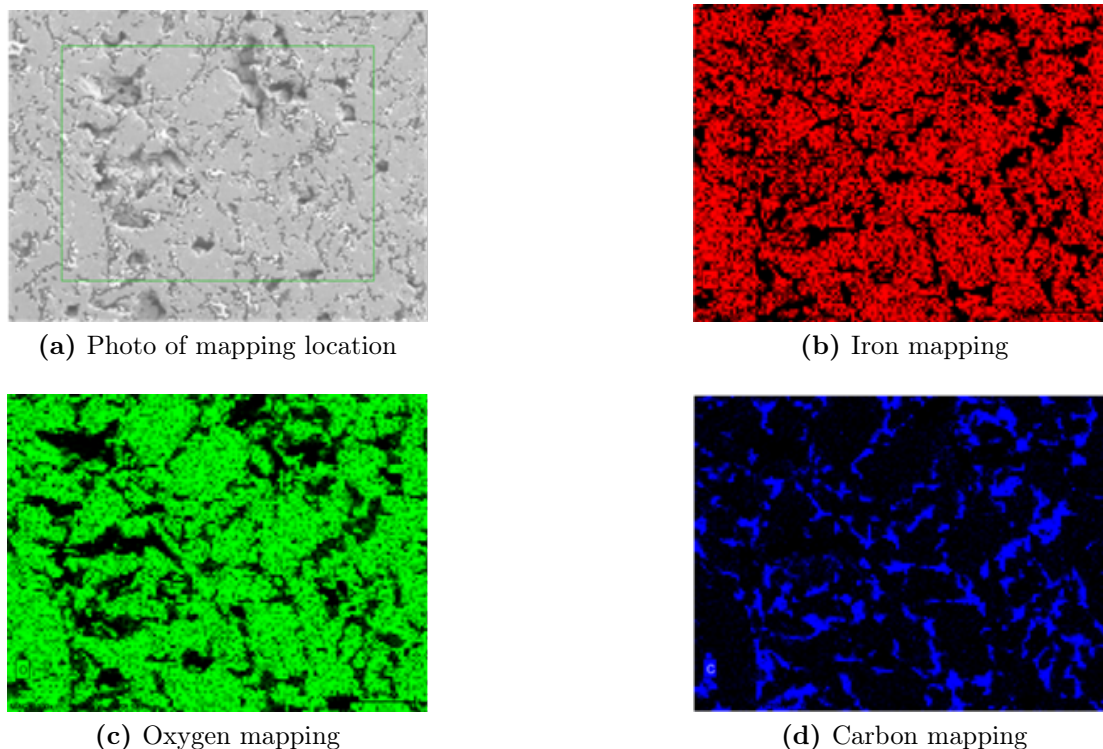


Figure 5.1.5: Elemental mapping of the TGA-sample. 1000x scale.

5.2 Experimental method 2 - High Temperature Vacuum Furnace

A calibration was performed on the furnace to determine the accuracy of the thermocouple. The theoretical melting point of copper is 1085 °C. The measure temperature when the copper melted in the furnace was 1215 °C. This means that the experiments were done with temperatures 130 °C lower than intended. The intended temperatures were 700 °C, 800 °C and 900 °C, but the actual temperatures were 570 °C, 670 °C and 770 °C. To make up for the difference, an extra carburisation experiment was done at 800 °C, adjusted for the deviation of the thermocouple.

The analysis of reduced samples started with the SEM picture results. As seen in Figure 5.2.1 (a), (b), and (c), a notable outcome is a partial increase in porous regions as the temperature increases, likely linked to an accelerated reduction rate at higher temperatures. Compared to the unreduced sample in Figure 5.1.2, the reduced samples have a visibly higher porosity.

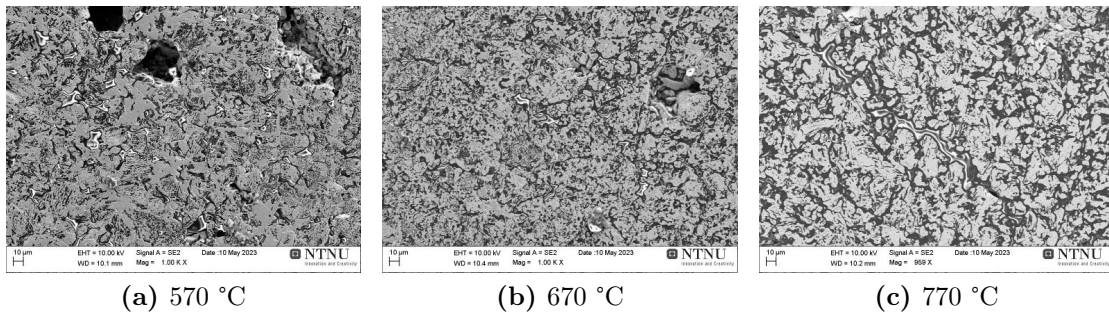


Figure 5.2.1: Surface structure of reduced samples. 1000x scale

When examining the oxygen concentrations, due to the porosity, conflicting results arise. Figure 5.2.2 and 5.2.3 showcase a decrease in oxygen concentration in the samples reduced at 570 °C and 670 °C. This is expected due to the reduction rate that correlates with oxygen loss.

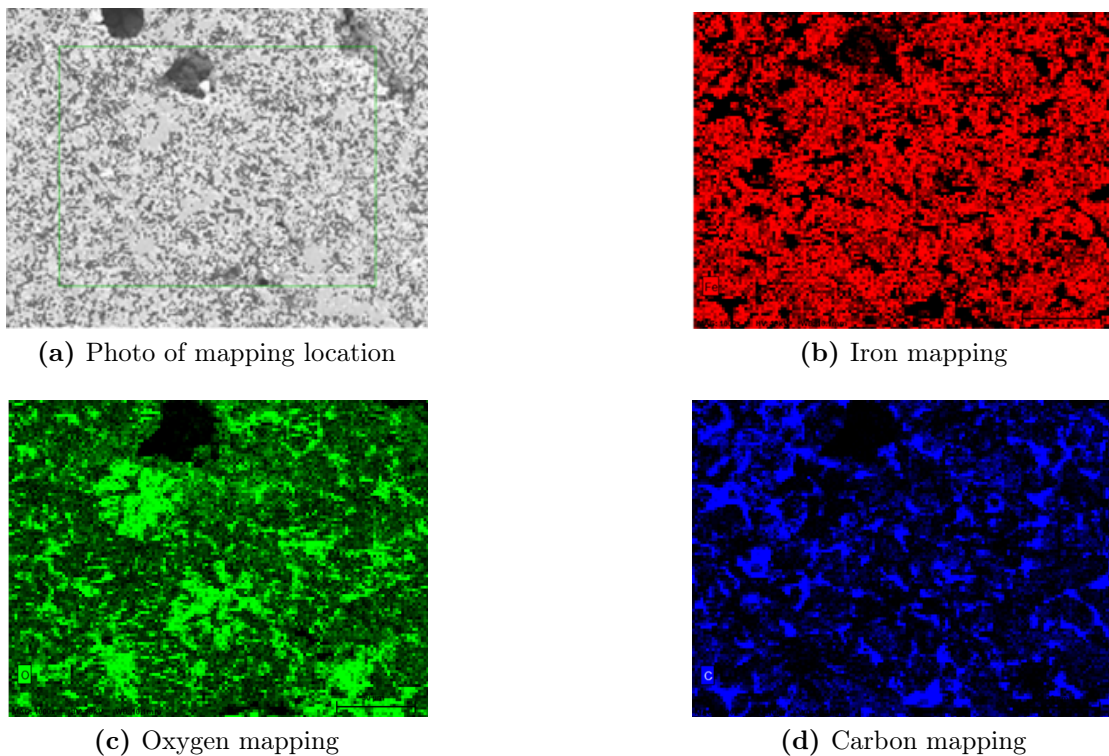
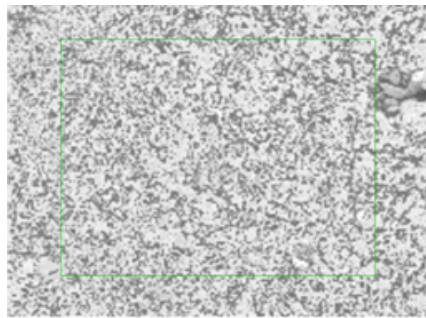
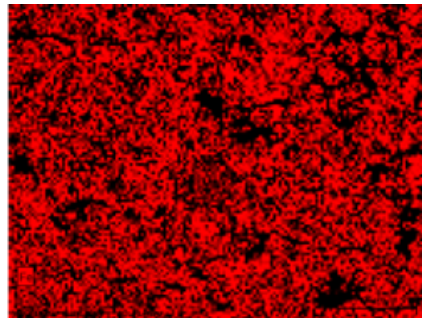


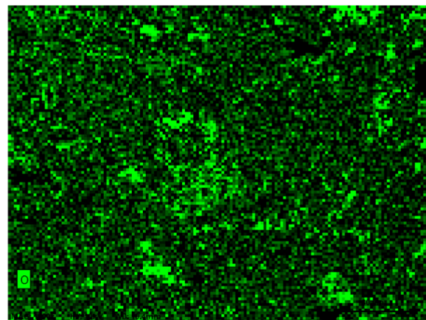
Figure 5.2.2: Elemental mapping of the 570 °C reduced sample from the vacuum furnace. 1000x scale.



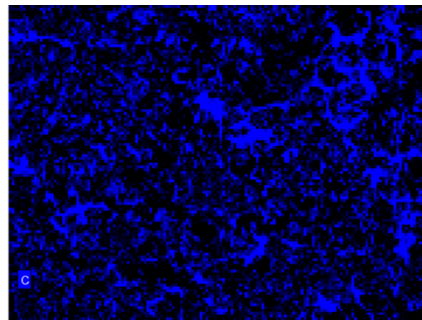
(a) Photo of mapping location



(b) Iron mapping



(c) Oxygen mapping



(d) Carbon mapping

Figure 5.2.3: Elemental mapping of the 670 °C reduced sample from the vacuum furnace. 1000x scale.

However, Figure 5.2.4 displays a sudden and unexpected increase in oxygen concentration at higher temperatures, compared to the samples at lower temperatures. A possible reason for this could be that the sample has re-oxidized to a certain degree from the atmosphere, before analysis was performed.

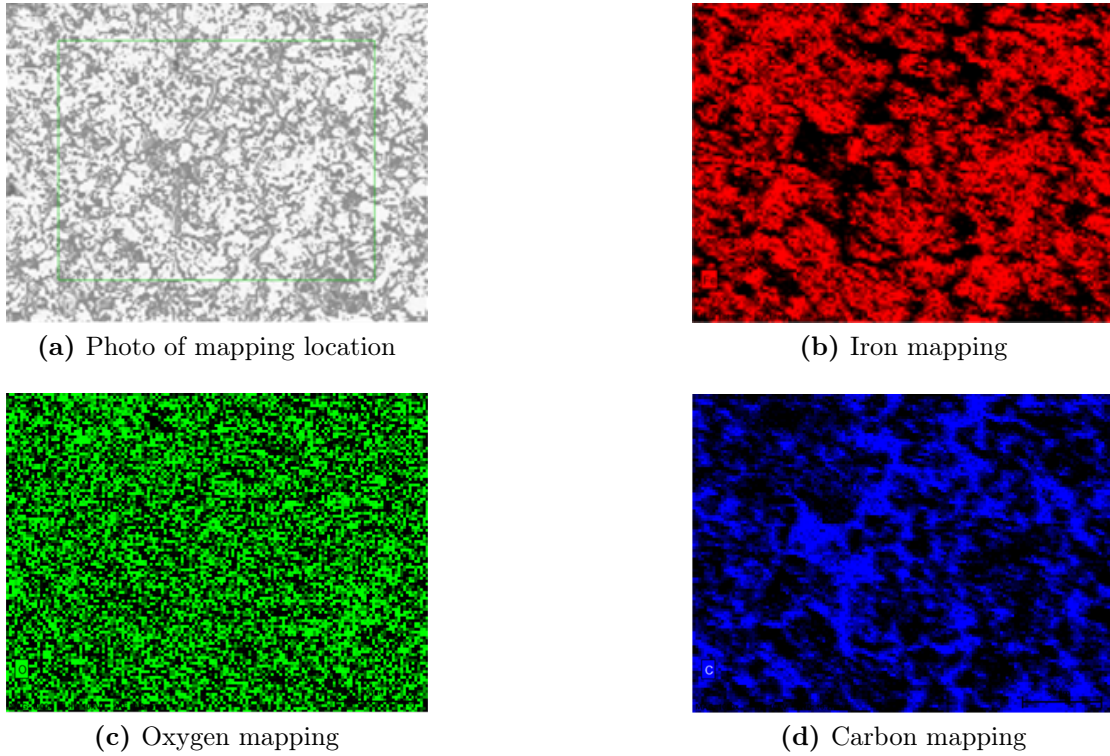


Figure 5.2.4: Elemental mapping of the 770 °C reduced sample from the vacuum furnace. 1000x scale.

For the samples that were both reduced and carburised, the most interesting result is shown in Figure 5.2.5 (a). This figure showcases an uncarburised core at 570 °C.

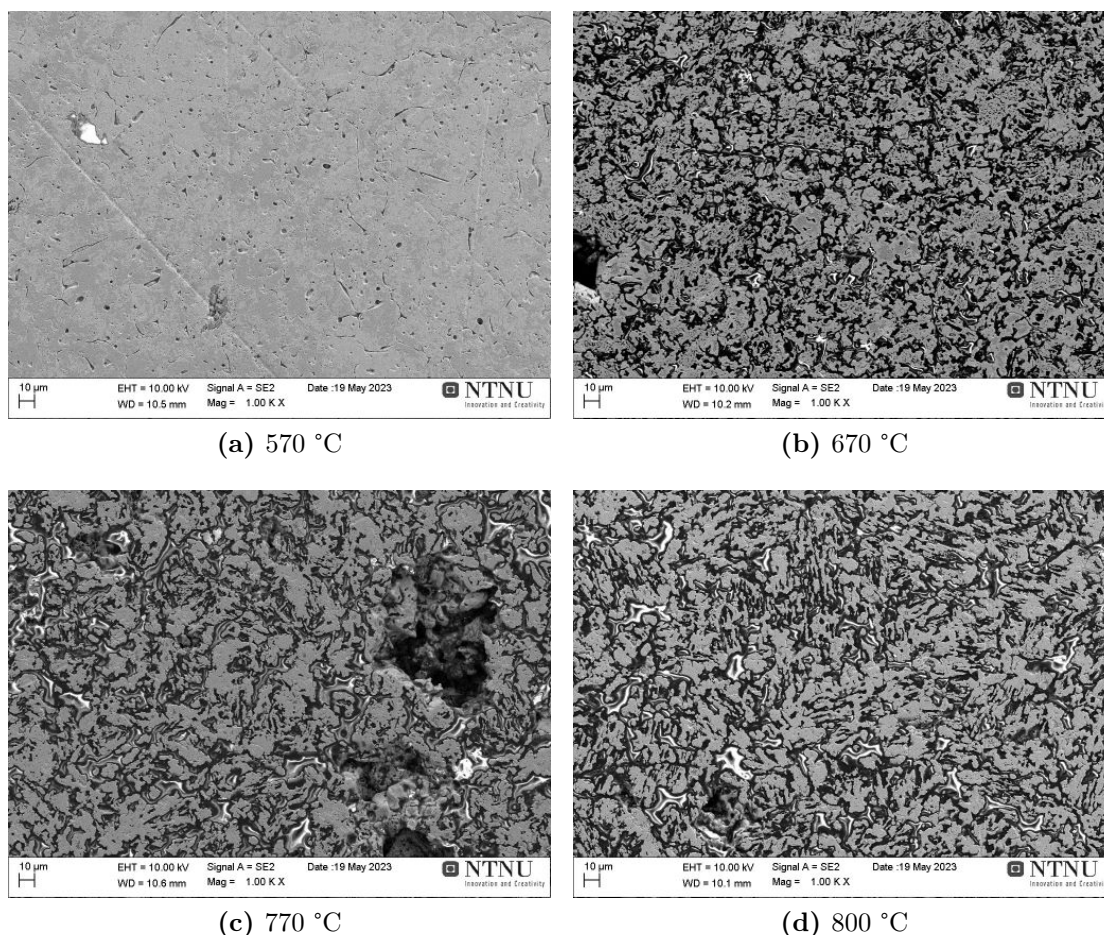


Figure 5.2.5: Surface structure of both reduced and carburised samples. 1000x scale.

Further exploration of the carburisation of the 570 °C sample is provided in Figure 5.2.6 through elemental mapping. It shows a smaller amount of both iron and oxygen, and a larger amount of carbon in the outer layer on the left, compared with the composition of the core to the right. This circumstance was partly expected, because the reason for this occurrence must be because the temperature has been too low to ensure complete carburisation. The degree of porosity in the inner layer was also lower than the outer layer, bearing a similar pattern to the unreduced sample as shown in Figure 5.1.2.

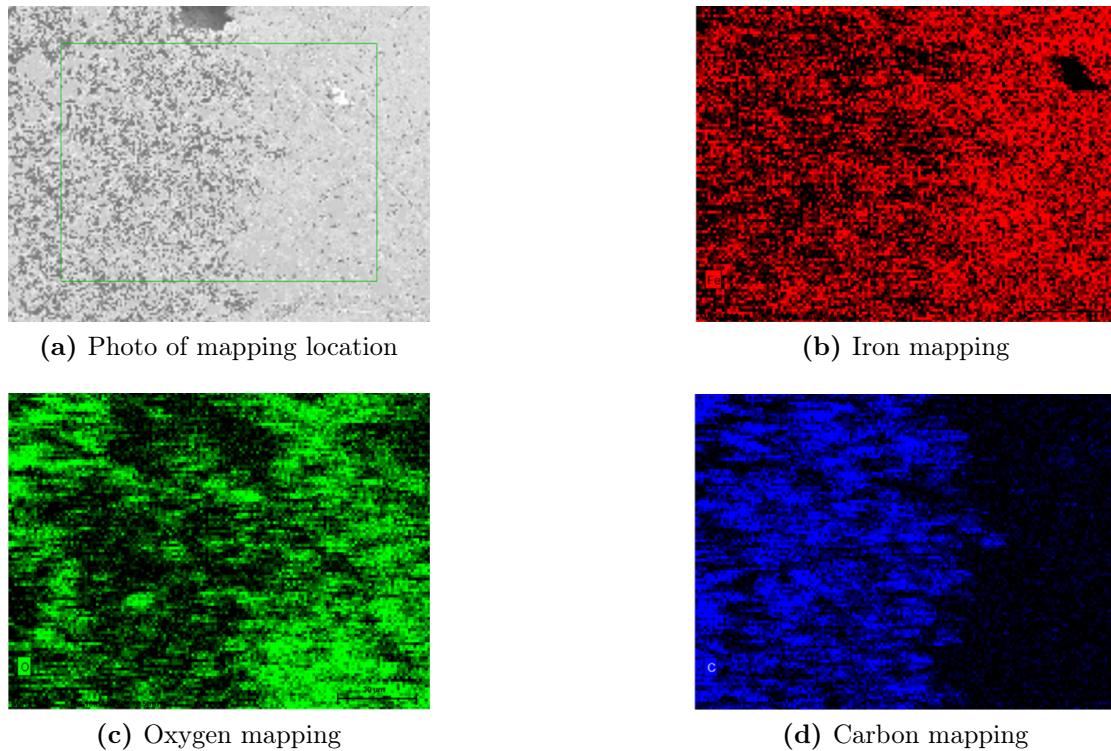


Figure 5.2.6: Elemental mapping of the 570 °C carburised sample from the vacuum furnace. 1000x scale.

Regarding temperatures above 670 °C, carburisation of the samples is apparent. As Figure 5.2.7, 5.2.8, and 5.2.9 demonstrate, carbon detection and its intensity increase with temperature, which is expected. This proves that temperatures above 670 °C are suitable for carburisation with methane. Temperatures below 670 °C are not suitable. As to which temperature is optimal, there is no notable difference for the samples above 670 °C, which might be because the holding time is long enough for the reaction to be complete. At shorter holding times, the results might be different, as higher temperatures generally has a higher rate of conversion from hematite to iron. Optimal temperatures for this thesis is therefore temperatures above 670 °C.

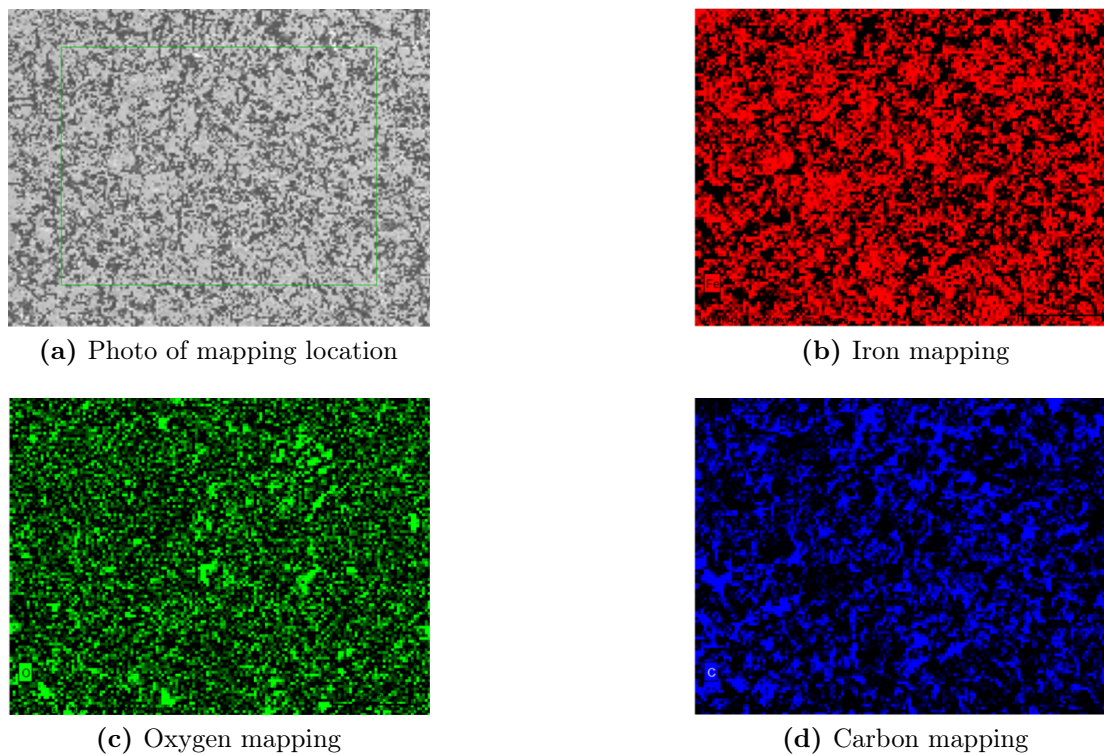


Figure 5.2.7: Elemental mapping of the 670 °C carburised sample from the vacuum furnace. 1000x scale.

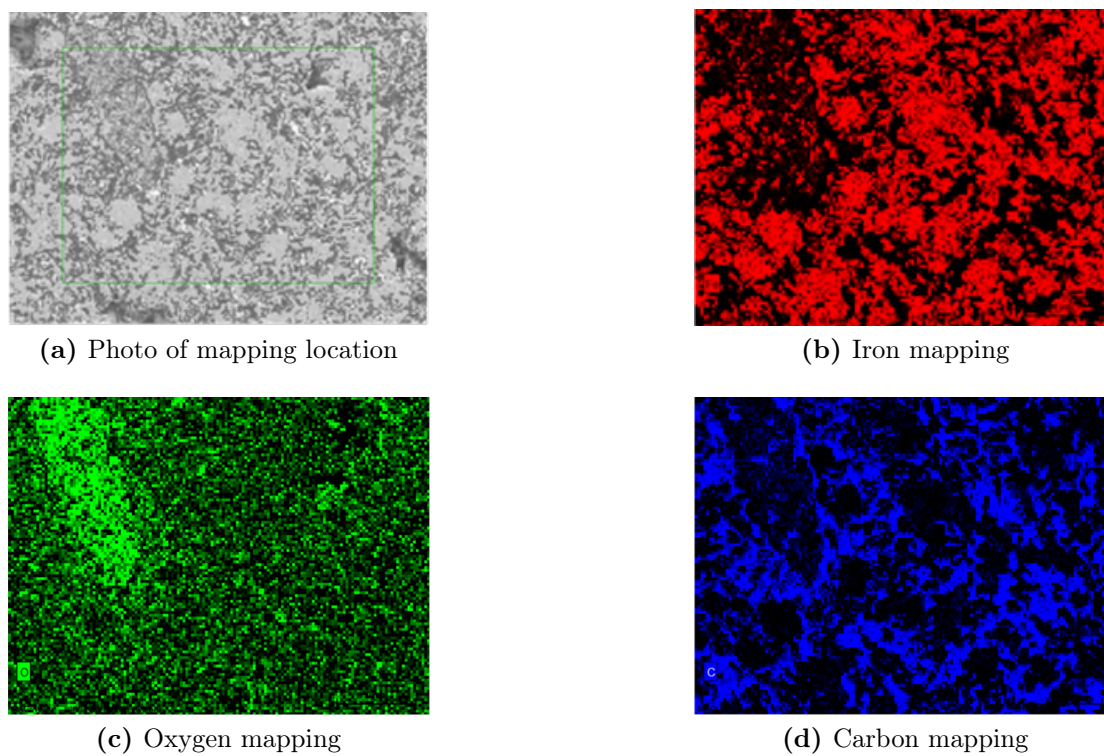


Figure 5.2.8: Elemental mapping of the 770 °C carburised sample from the vacuum furnace. 1000x scale.

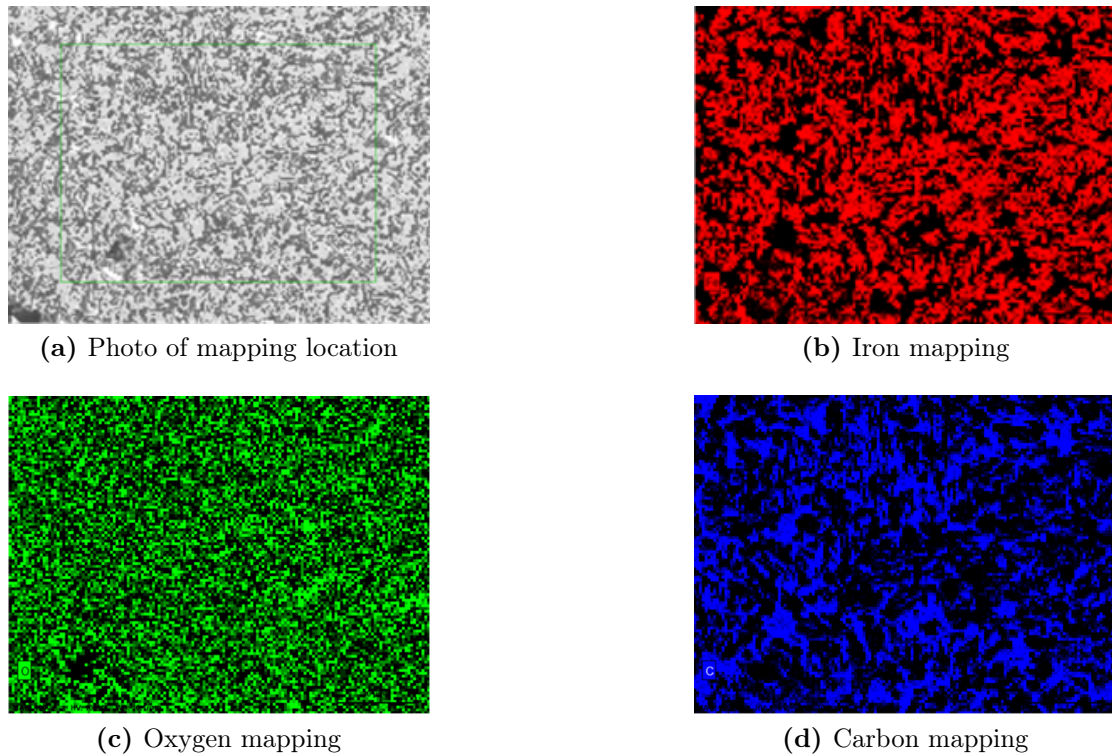
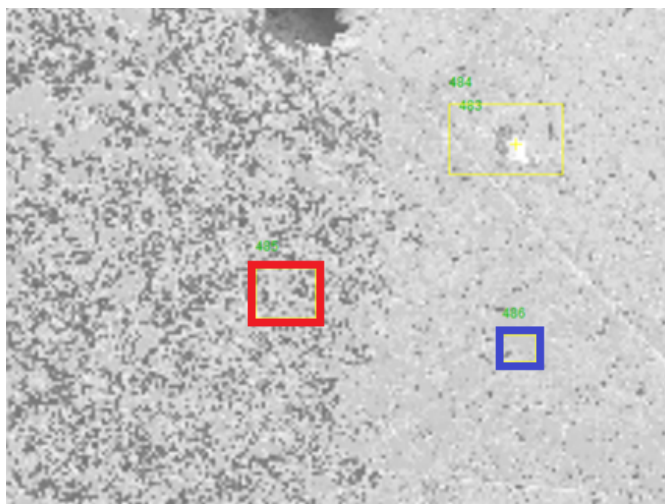
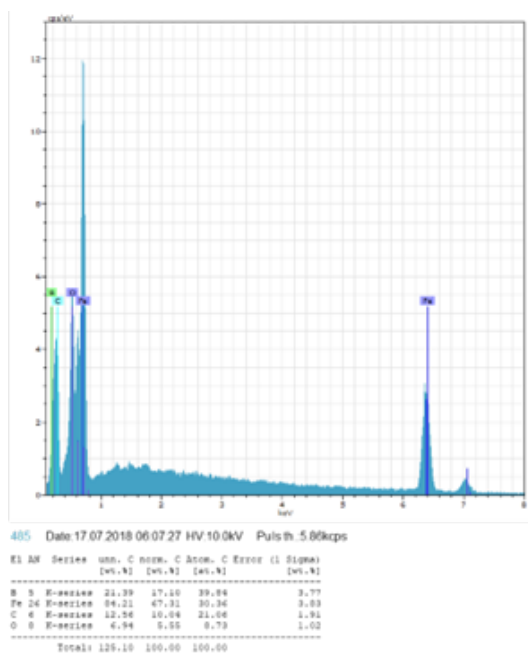


Figure 5.2.9: Elemental mapping of the 800 °C carburised sample from the vacuum furnace. 1000x scale.

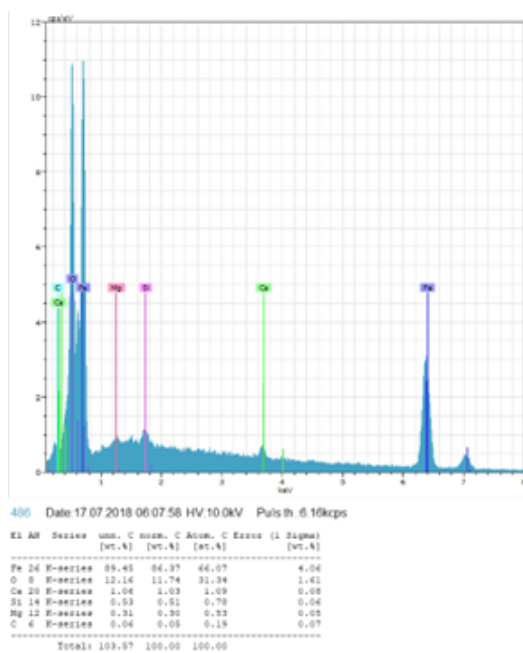
For the sample that was not fully carburised, an EDS analysis was done, as shown in Figure 5.2.10. The readings in (b) are for the outer layer and it detected an iron amount of 67.31%, an oxygen amount of 5.55%, and a carbon amount of 10.04%. The inner layer is analysed in (c), and shows an iron amount of 86.37%, oxygen amount of 11.74%, and carbon amount of just 0.05%. The temperature used in this case must have been too low to ensure complete carburisation. A smaller rate of carburisation is expected in lower temperatures, which must have happened in this case. This assumption was further proved by the previously shown results regarding SEM photos and elementary mapping in Figure 5.2.5 and 5.2.6. The pellet is a great example of shrinking core in action, as the outer layer has been processed, but the inner layer, the core, is untouched. Further EDS analyses are added in Appendix B.



(a) The area in which the EDS analysis was taking place.



(b) EDS analysis of the red area.



(c) EDS analysis of the blue area.

Figure 5.2.10: EDS analysis of the surface of a sample reduced and carburised at 570 °C in high-temperature vacuum furnace.

5.3 HSC Chemistry 9

To use the Equilibrium composition module, the initial amounts needed to be calculated. This is detailed in Appendix C. The results are shown in Figure 5.3.1.

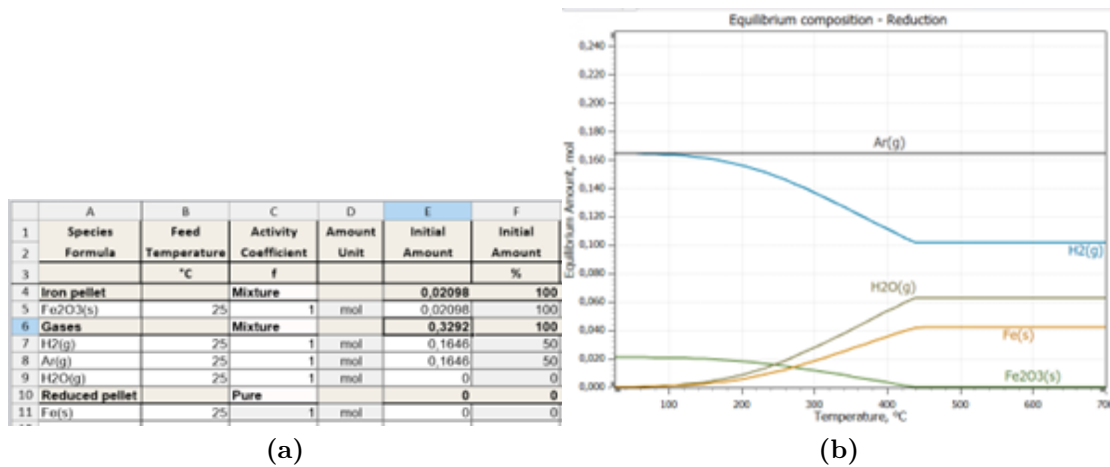


Figure 5.3.1: The equilibrium composition of the reduction

According to the graph, the reduction starts happening already at about 150 °C and at around 400 °C the reaction stops. The results show that the final amount of iron is 0.04196 mol, which is twice the amount of iron oxide. This means that all the original iron oxide has been reduced to iron. There are a few factors to consider when looking at the graph. First, the Equilibrium Composition-module assumes equilibrium at every temperature. This is probably not what happens, especially with the furnace experiments. There, the temperature rate is quite high, 100 °C/min, so the reactions will not have time to reach equilibrium. The furnace is also not a closed system, as gas is supplied and removed constantly throughout the process. Additionally, all pellets will contain a certain level of inhomogeneity, something the software does not account for. In view of this, the simulations are still in good agreement with the experimental results, detailed in 5.1.

The carburisation results are shown in Figure 5.3.2.

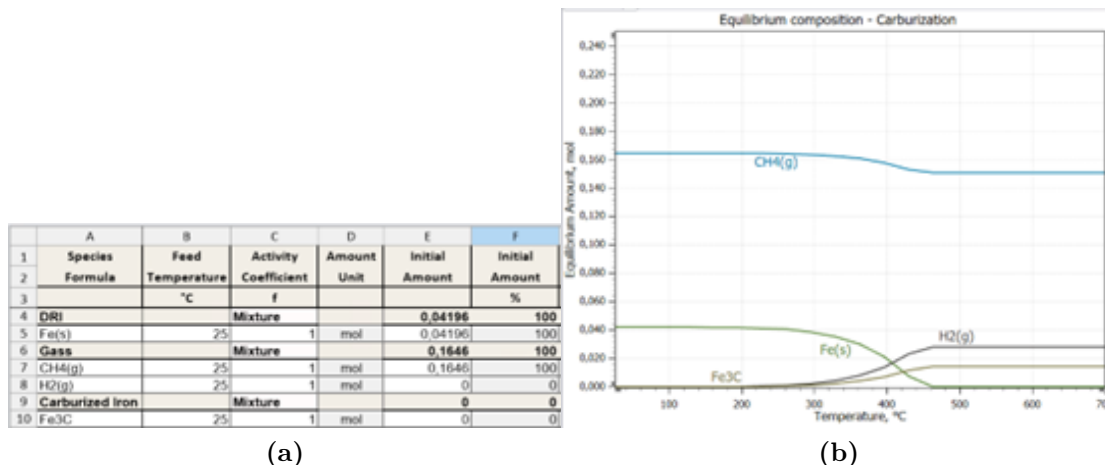


Figure 5.3.2: The equilibrium composition of the carburisation

Here, the process starts at around 300 °C and ends at 450 °C, where all of the iron has reacted with carbon to be carburised. In the experiments with the high-temperature vacuum furnace, the iron ore pellet carburised at 570 °C was not fully carburised, so the simulation is, in this case, not in agreement with the results. In addition to the problems listed for the reduction example, the carburisation example also has a problem with the temperature. When doing an experiment with the furnace, the carburisation process takes place during the cooling phase, but the module does not allow for temperatures to go from high to low. The graph will therefore not be accurate.

SUMMARY & CONCLUSIONS

The present work's purpose was to investigate the optimum temperature for reducing iron ore pellets in H_2 gas at varying temperatures (570 °C, 670°C and 770°C). The iron ore pellets were further carburised in an atmosphere of CH_4 gas. The reduction and carburisation processes was simulated in a software called HSC Chemistry.

The experiments were performed using a high-temperature vacuum furnace, and it resulted in iron ore pellets that showed increased porosity, indicating that the reduction process had been initiated. Most of the reduced pellets also showed a decrease in oxygen concentration at the surface. The exception was the iron ore pellet reduced at 770 °C, which might possibly be due to reoxidation of the pellet surface before analysis. The iron ore pellets carburised at 670 °C and 770 °C showed a complete carburisation, but the sample carburised at 570 °C showed that only the outer layers had been carburised. In conclusion, 570 °C is too low for obtaining a complete carburisation.

The simulations using HSC Chemistry 9 showed that the iron ore pellets would be completely reduced and carburised with the given parameters. The program assumes equilibrium at every step, and the iron ore pellets will contain a certain level of inhomogeneity. Therefore, the simulations can only give indications of what can be obtained. In view of this, the simulation results were in good agreement with the overall outcome of the experimental work.

FUTURE WORK

The initial goal was to primarily utilise a Thermogravimetric Analyser (TGA) to process our samples. However, due to an unforeseen equipment malfunction, the high-temperature vacuum furnace method had to become our primary means to get samples. For future experiments, it would be best to carry out the experiments on TGA, given its superior ability to control temperature, and its built-in microscale to record the mass change of the pellet. In general, it is best suited to run reduction and carburisation experiments.

Additionally, it would be interesting to test samples with alternative carburising gases, for example carbon monoxide. The aim would be to directly compare the efficacy of methane and carbon monoxide as carburising gases. Both gases, in theory, should serve adequately in performing carburisation. However, a side-by-side comparison would provide a definitive answer to which one is most effective.

Regarding the high-temperature vacuum furnace experiments, the tests were performed at peak temperatures of 570°C, 670°C, 770°C, and 800°C using only hydrogen gas. It would be of interest to broaden the temperature variety. Exploring higher temperatures could provide more information into how these temperatures affect the samples. It might also be beneficial to examine how varying the hold time at peak temperature would affect the reduction and carburisation processes. All samples in this experiment were held at peak temperature for 160 minutes. At an optimal temperature, this time could potentially be cut shorter. Lastly, it is possible to perform the reduction in CO gas as well. Varying the gas composition in the furnace atmosphere might affect the reduction process.

REFERENCES

- [1] F. Bradley . “December 2022 crude steel production and 2022 global crude steel production totals”. In: (Jan. 2023). URL: <https://worldsteel.org/media-centre/press-releases/2023/december-2022-crude-steel-production-and-2022-global-totals/> (visited on June 8, 2023).
- [2] Z. Fan. and J. Friedmann. “Low-Carbon Production of Iron & Steel: Technology Options, Economic Assessment, and Policy”. In: (Mar. 2021). URL: <https://www.energypolicy.columbia.edu/publications/low-carbon-production-iron-steel-technology-options-economic-assessment-and-policy/>.
- [3] Dolf Gielen. “CO2 removal in the iron and steel industry”. In: *Energy conversion and management* 44.7 (2003), pp. 1027–1037.
- [4] L.R. López et al. “CO2 in indoor environments: From environmental and health risk to potential renewable carbon source”. In: *Science of The Total Environment* 856 (2023), p. 159088. ISSN: 0048-9697. DOI: <https://doi.org/10.1016/j.scitotenv.2022.159088>. URL: <https://www.sciencedirect.com/science/article/pii/S0048969722061873>.
- [5] “Total production of crude steel. World total 2022”. In: (Mar. 2023). URL: https://worldsteel.org/steel-topics/statistics/annual-production-steel-data/?ind=P1_crude_steel_total_pub/CHN/IND (visited on June 8, 2023).
- [6] F. Bradley . “worldsteel Short Range Outlook October 2022”. In: (Oct. 2022). URL: [https://worldsteel.org/media-centre/press-releases/2022/worldsteel-short-range-outlook-october-2022/#:~:text=The%20World%20Steel%20Association%20\(worldsteel,1.0%25%20to%20reach%201%2C814.7%20Mt./](https://worldsteel.org/media-centre/press-releases/2022/worldsteel-short-range-outlook-october-2022/#:~:text=The%20World%20Steel%20Association%20(worldsteel,1.0%25%20to%20reach%201%2C814.7%20Mt./) (visited on June 8, 2023).
- [7] F. Bradley . “Short Range Outlook April 2023. Steel demand, finished steel”. In: (Apr. 2023). URL: <https://worldsteel.org/steel-topics/statistics/short-range-outlook/> (visited on June 8, 2023).
- [8] TK Sandeep Kumar et al. “Fossil-Free Carburization of Hydrogen-Based DRP”. In: (2023), pp. 145–150.
- [9] *The UN and Sustainability*. 2023. URL: <https://www.un.org/en/about-us/un-and-sustainability#:~:text=The%202020%20Report%20found%20the,came%20from%20staff%20air%20travel>. (visited on June 8, 2023).

- [10] “Hydrogen in steel production: what is happening in Europe – part two”. In: (May 2021). URL: <https://bellona.org/news/eu/2021-05-hydrogen-in-steel-production-what-is-happening-in-europe-part-two> (visited on June 8, 2023).
- [11] A. Odenweller et al. “Probabilistic feasibility space of scaling up green hydrogen supply”. In: *Analyst* (2022). DOI: 10.1038/s41560-022-01097-4. URL: <https://www.pik-potsdam.de/en/news/latest-news/green-hydrogen-short-term-scarcity-long-term-uncertainty> (visited on June 8, 2023).
- [12] Beheshti. R. *Sustainable Aluminium and Iron Production*. 2017.
- [13] Robert Donald Walker. *Ores*. URL: <https://www.britannica.com/technology/iron-processing/Ores> (visited on May 30, 2023).
- [14] Chris Barrington. *Pig iron production - blast furnace route*. Jan. 2021. URL: <https://www.metallics.org/pig-iron-bf.html> (visited on June 1, 2023).
- [15] *How Does A Blast Furnace Work?* July 2018. URL: <https://www.mbrashem.com/how-does-a-blast-furnace-work/> (visited on June 1, 2023).
- [16] Sujay Kumar Dutta and Rameshwar Sah. “Direct reduced iron: Production”. In: *Encyclopedia of Iron, Steel, and Their Alloys* (Mar. 2016), pp. 1082–1108. DOI: 10.1081/e-eisa-120050996.
- [17] Basak Anameric and S. Komar Kawatra. “Properties and features of direct reduced iron”. In: *Mineral Processing and Extractive Metallurgy Review* 28.1 (2007), pp. 59–116. DOI: 10.1080/08827500600835576.
- [18] Donn Saylor. *What is direct reduced iron?* June 2023. URL: <https://www.aboutmechanics.com/what-is-direct-reduced-iron.htm> (visited on May 30, 2023).
- [19] T. K. Kumar et al. “Carburization behavior of hydrogen-reduced DRI using synthetic bio-syngas mixtures as fossil-free carbon sources”. In: *Journal of Sustainable Metallurgy* 8.4 (Sept. 2022), pp. 1546–1560. DOI: 10.1007/s40831-022-00590-0.
- [20] J Szekely, JW Evans, and HY Sohn. “Gas-solid reactions 1976”. In: *New York, Academic Press*. ().
- [21] Fabrice Patisson and Olivier Mirgaux. “Hydrogen ironmaking: How it works”. In: *Metals* 10.7 (July 2020), p. 922. DOI: 10.3390/met10070922.
- [22] B. Monsen et al. “Characterization of DR Pellets for DRI Applications”. In: May 2015, p. 5.
- [23] Paul Gabbott. *Principles and applications of thermal analysis*. John Wiley & Sons, 2008, pp. 88–89.
- [24] Rod Bottom. “Thermogravimetric analysis”. In: *Principles and applications of thermal analysis* 1.906 (2008), pp. 87–118.
- [25] Charles Mansfield Earnest. *Compositional analysis by thermogravimetry*. Vol. 997. ASTM International, 1988, p. 148.

- [26] A. W. Coats and J. P. Redfern. “Thermogravimetric analysis. A review”. In: *Analyst* 88 (1053 1963), pp. 906–924. DOI: 10.1039/AN9638800906. URL: <http://dx.doi.org/10.1039/AN9638800906>.
- [27] F Jahan and MJ Ballico. “Annealing state dependence of the calibration of type R and type S thermocouples”. In: *International Journal of Thermophysics* 31 (2010), pp. 1544–1553.
- [28] O Ongrai et al. “A miniature high-temperature fixed point for self-validation of type C thermocouples”. In: *Measurement Science and Technology* 22.10 (2011), p. 105103.
- [29] Smith. O and Pharm. B. “Limitations of Optical Microscopy”. In: (Aug. 2018). URL: <https://www.news-medical.net/life-sciences/Limitations-of-Optical-Microscopy.aspx#:~:text=The%20maximum%20magnification%20that%20can,be%20achieved%20with%20electron%20microscopy>. (visited on June 8, 2023).
- [30] *What is Scanning Electron Microscopy?* URL: <https://www.jeolusa.com/RESOURCES/Electron-Optics/Scanning-Electron-Microscopy-Basics> (visited on June 8, 2023).
- [31] Smith. O and Pharm. B. “History of the Electron Microscope”. In: (Aug. 2018). URL: <https://www.news-medical.net/life-sciences/History-of-the-Electron-Microscope.aspx> (visited on June 8, 2023).
- [32] *Zeiss Ultra 55*. URL: <https://www.felmi-zfe.at/instrumentation/sem/zeiss-ultra-55/> (visited on June 8, 2023).
- [33] *Scanning Electron Microscopy: 6 SEM Sample Preparation Pointers for Successful Imaging*. Dec. 2021. URL: <https://bitesizebio.com/34150/sem-sample-prep/#:~:text=So%2C%20metal%20samples%20require%20no,layer%20of%20gold%20works%20fine>. (visited on June 8, 2023).
- [34] Nanakoudis. A. *SEM: Types of Electrons and the Information They Provide*. Nov. 2019. URL: <https://www.thermofisher.com/blog/materials/sem-signal-types-electrons-and-the-information-they-provide/#:~:text=Comparison%20of%20SEM%20signals,material%20appears%20in%20the%20image>. (visited on June 8, 2023).
- [35] Phuc D Ngo. “Energy dispersive spectroscopy”. In: *Failure analysis of integrated circuits: Tools and techniques* (1999), pp. 205–215.
- [36] *SEM: Types of Electrons and the Information They Provide*. URL: <https://cmrf.research.uiowa.edu/scanning-electron-microscopy> (visited on June 8, 2023).
- [37] *HSC Chemistry*. en. URL: <https://www.mogroup.com/portfolio/hsc-chemistry/> (visited on June 1, 2023).

APPENDICES

APPENDIX A - SAMPLE PREPARATION

A1 - Epoxy casting

Equipment:

- Struers CitoVac Vacuum Impregnation Unit
- Struers Minitom cutting machine
- Epoxy sample holders
- Single use beaker
- Stir stick

Chemicals:

- Korasilon Silicon paste
- Epofix hardener
- Epofix resin

The inside wall of the epoxy sample holder was smeared with Korasilon paste, which made it easier to remove the samples after the epoxy had stiffened. The epoxy was made by mixing the Epofix hardener and Epofix resin in a single-use beaker. The mixture was thoroughly stirred and vacuumed before use. The samples were individually put inside their epoxy sample holder and then covered in the epoxy mixture. All samples were cast with epoxy the same way. The stiffening time was about 24 hours. After the epoxy was stiffened, the samples were removed from the epoxy sample holders. The cast samples were then cut in half with a saw to give accessibility to the core of the sample. Each half of the sample was cast again, with the core of the sample accessible.

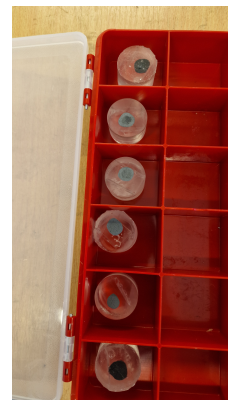


Figure A.1: Picture of the samples casted in epoxy.

A2 - Polishing

Equipment:

- Struers TegraPol-31 semi-automatic grinding and polishing machine
- Magnetic disc
- SiC grinding papers, grit #220, #800, #1200, #2400, #4000
- Nap polishing cloth, 1 μm
- Ultrasonic bath

Chemicals:

- Ethanol
- Polishing soap
- Zalo

The grinding and polishing of the samples were performed with a semi-automatic machine. A magnetic disc was placed on the spinning wheel, and the grinding papers used were placed on the disc. The grit of the papers used was, in order: #220, #800, #1200, #2000 and #4000. The samples were placed in a mount attached to the machine, and the machine was started. Each polish took 2.5 min. After polishing, the samples were thoroughly washed with polishing soap and water. For grits #1200 and higher, the papers were coated in polishing soap, and after the polishing and washing, the samples were placed in beakers filled with ethanol and placed in an ultrasonic bath to remove all contaminations. After using grit #4000, the samples were polished one last time with a 1 μm nap polishing cloth.

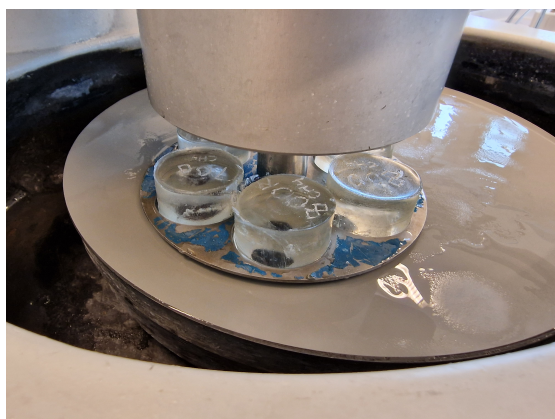
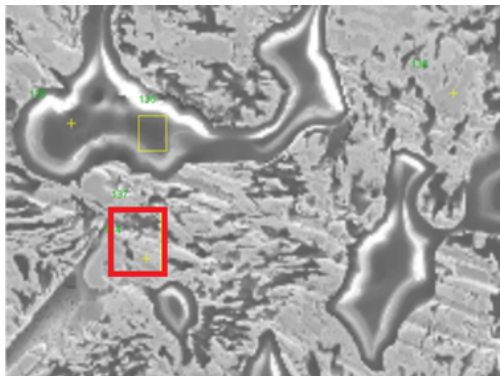


Figure A.2: Picture of the samples being polished in the automatic grinding and polishing machine.

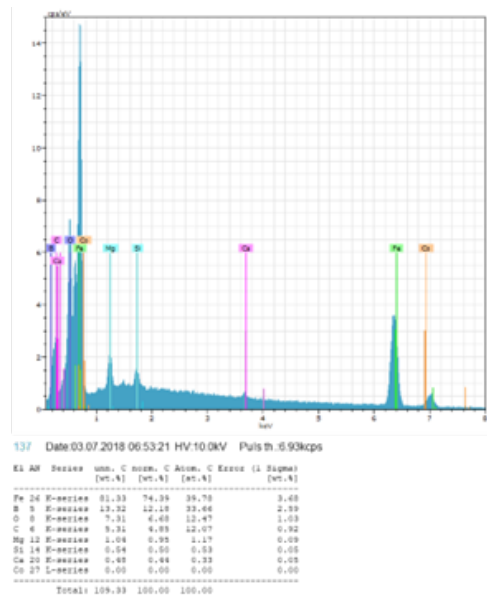
APPENDIX B - SEM/EDS ANALYSIS

In addition to elemental mapping, various Energy-Dispersive X-ray Spectroscopy (EDS) analyses were performed on the samples to determine the number of multiple elements present at specific points on the surface of the sample. It should, however, be mentioned that the obtained analysis result might represent only some of the pellets in question due to their inhomogeneity. The EDS results gave only the composition at a small area of the sample surface.

The results of the quantitative EDS readings on the reduced samples are shown in Figures B.1, B.2, and B.3. The fluctuation in oxygen (O) concentration increased from 6.68% at 570 °C to a spike of 18.44% at 670 °C, before decreasing again to 2.18% at 770 °C. These readings also revealed unexpected fluctuations in the iron (Fe) concentration at 570 °C and 770 °C. Likewise, for the same reasons as the elemental mapping results, the area set for EDS analysis could have been inflicted with re-oxidation, hence the sudden intense oxygen concentration.

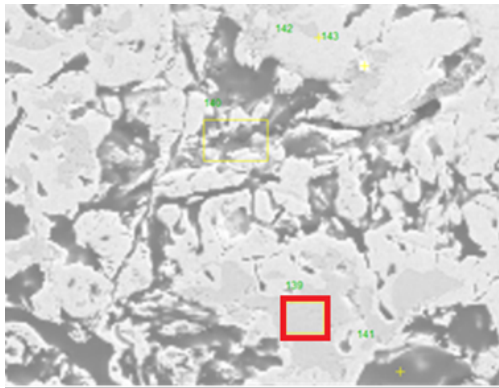


(a) The area in which the EDS analysis was performed.

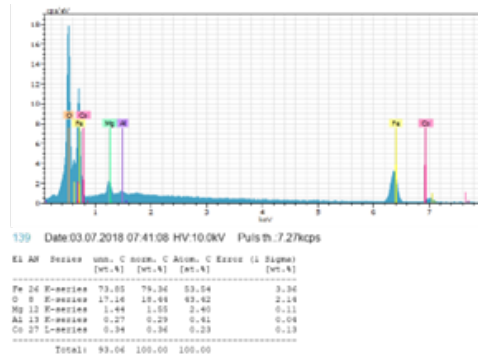


(b) The EDS analysis.

Figure B.1: EDS analysis of the surface of an iron ore pellet reduced at 570 °C in a high-temperature vacuum furnace.



(a) The area in which the EDS analysis was performed.

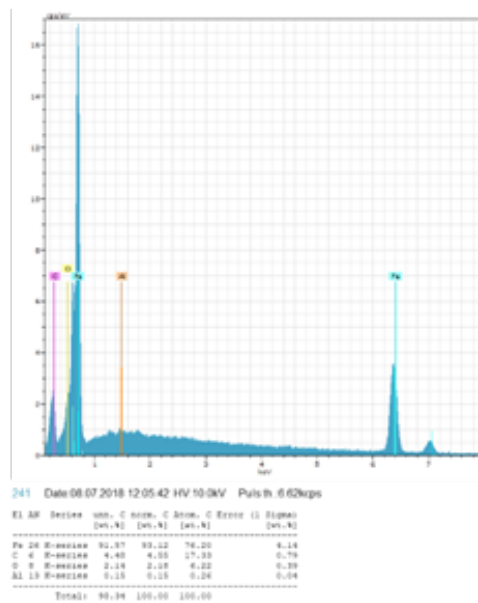


(b) The EDS analysis.

Figure B.2: EDS analysis of the surface of an iron ore pellet reduced at 670 °C in a high-temperature vacuum furnace.



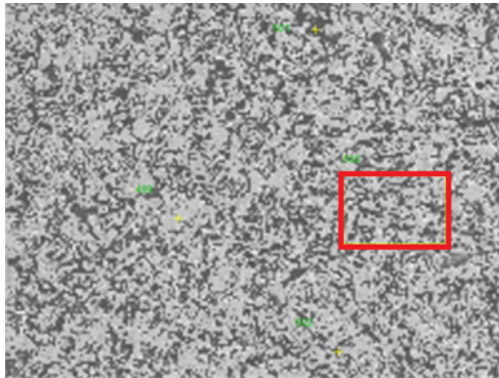
(a) The area in which the EDS analysis was performed.



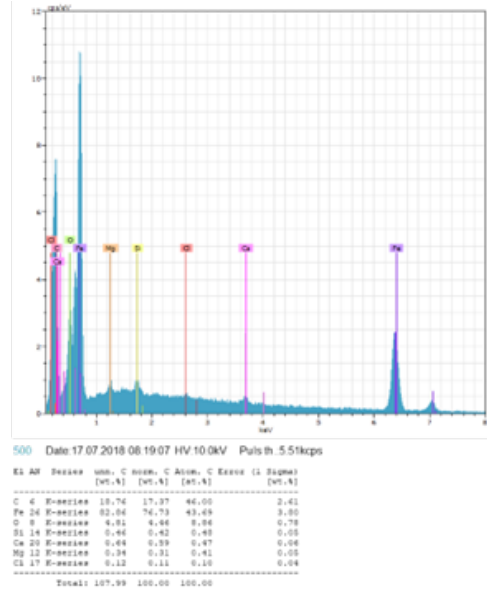
(b) The EDS analysis.

Figure B.3: EDS analysis of the surface of an iron ore pellet reduced at 770 °C in a high-temperature vacuum furnace.

The EDS readings for both the reduced and carbonised samples at 670 °C, 770 °C, and 800 °C, presented in Figures B.4, B.5, and B.6, indicate an increase in the percent of carbon mass with temperature, which corresponds well with the elemental mapping observations. This outcome was expected, as the carbon-rich gas interacted with the samples. This interaction also corresponds with the shrinking core model's prediction for carbonisation, thereby confirming the preliminary carbonisation results.

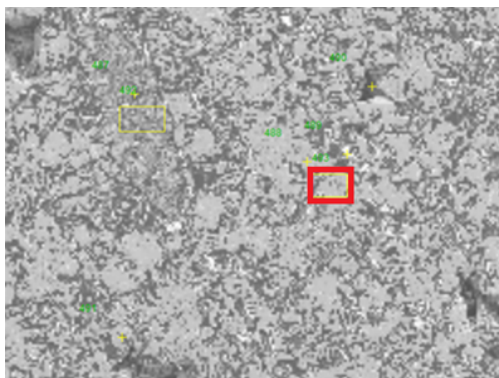


(a) The area in which the EDS analysis was performed.

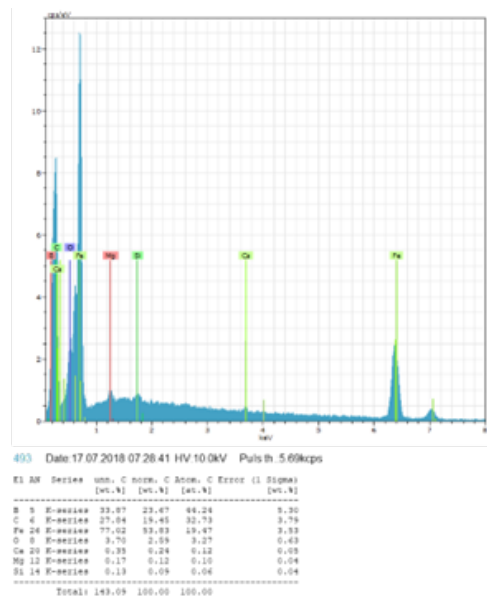


(b) EDS analysis.

Figure B.4: EDS analysis of the surface of an iron ore pellet reduced at 670 °C in a high-temperature vacuum furnace.

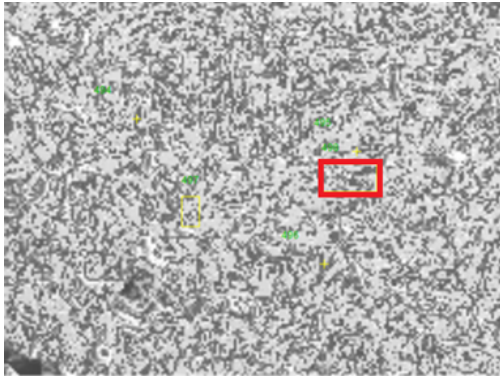


(a) The area in which the EDS analysis was performed.

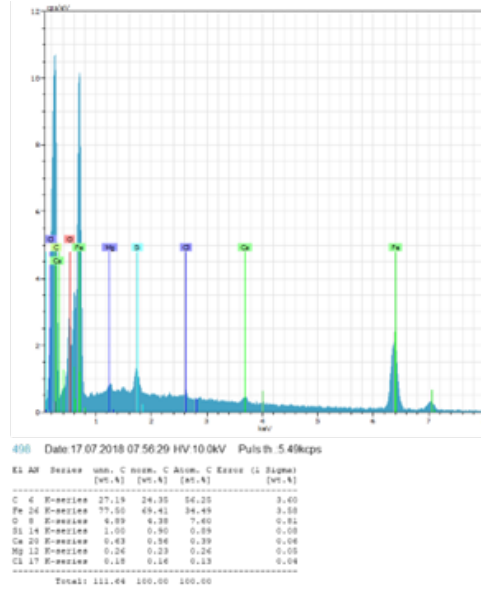


(b) EDS analysis.

Figure B.5: EDS analysis of the surface of an iron ore pellet reduced at 770 °C in a high-temperature vacuum furnace.



(a) The area in which the EDS analysis was performed.



(b) EDS analysis.

Figure B.6: EDS analysis of the surface of an iron ore pellet reduced at 800 °C in a high-temperature vacuum furnace.

APPENDIX C - HSC CHEMISTRY 9 CALCULATIONS

C1 - The Initial amount of gases

The high-temperature vacuum furnace used 5 minutes and 22 seconds to fill up with H₂ gas with a flow rate of 1,5 L/min. The volume of the furnace chamber is, therefore:

$$5.3667 \text{ min} * 1.5 \text{ L/min} = 8.05 \text{ L} \quad (1)$$

To translate that into mol, the ideal gas law was used. The temperature was 298 K, and the pressure was 1 atm.

$$n = \frac{PV}{RT} = \frac{1 \text{ atm} * 8.05 \text{ L}}{0.08205 \frac{\text{L*atm}}{\text{K*mol}} * 298 \text{ K}} = 0.3292 \text{ mol} \quad (2)$$

The gas used was a mixture of 50% H₂ and 50% Ar, so the amount of H₂ gas in the chamber was:

$$0.3292 \text{ mol} * 50\% = 0.1646 \text{ mol} \quad (3)$$

The amount of Ar was the same, i.e. 0.1646 mol.

C2 - The initial amount of hematite

The average weight of a pellet used in the furnace was 3.351 g. Hematite (Fe₂O₃) had a molar mass of 159.69 g/mol. An average pellet would, thereby, contain the following number of moles of Fe₂O₃:

$$n = \frac{3.351 \text{ g}}{159.69 \text{ g/mol}} \quad (4)$$